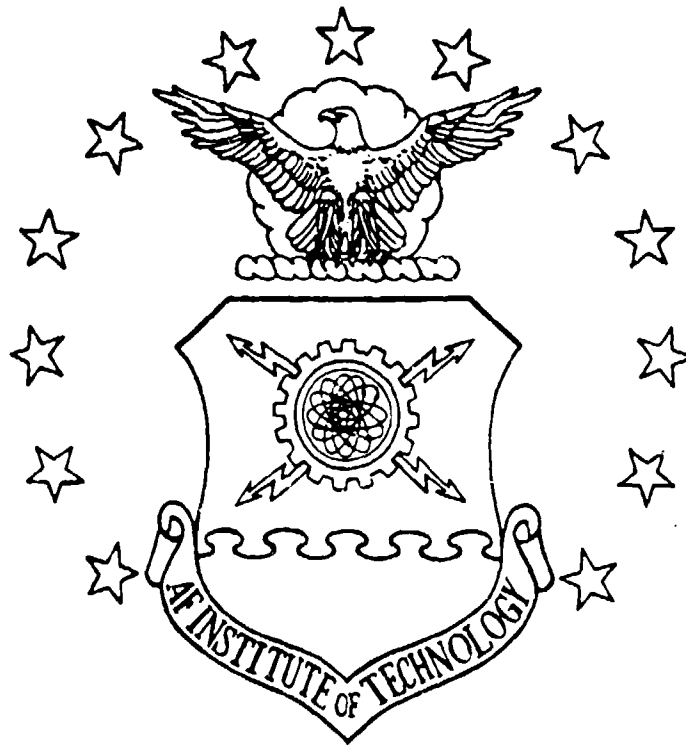
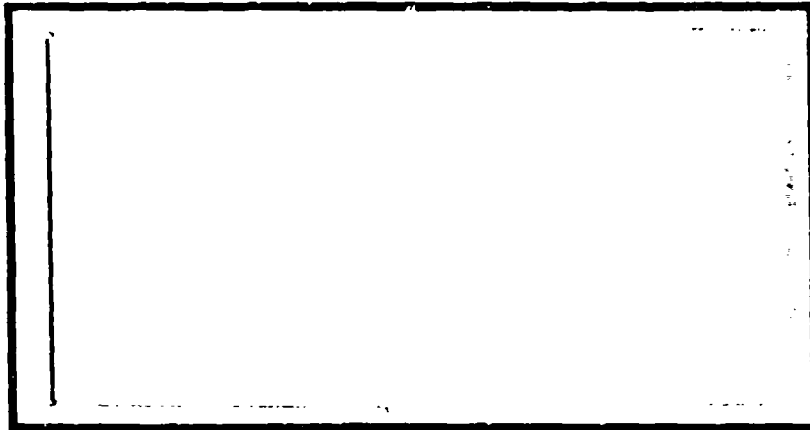


AD-A202 937



DTIC
 ELECTE
 JAN 17 1989
 SH



DEPARTMENT OF THE AIR FORCE
 AIR UNIVERSITY
AIR FORCE INSTITUTE OF TECHNOLOGY

Wright-Patterson Air Force Base, Ohio

DISTRIBUTION STATEMENT A
 Approved for public release;
 Distribution Unlimited

89 1 17 021

①

AFIT/GA/AA/88D-11

DTIC
ELECTE
JAN 17 1989
S D

H
8

EFFECT OF TWO-BODY MOTION ON RADAR
BEAM QUALITY FOR VARIOUS DISTRIBUTED
SPARSE ARRAY CONFIGURATIONS
THESIS

Michael G. Spencer
Captain, USAF

AFIT/GA/AA/88D-11

Approved for public release; distribution unlimited

AFIT/GA/AA/88D-11

EFFECT OF TWO-BODY MOTION ON RADAR BEAM QUALITY FOR VARIOUS
DISTRIBUTED SPARSE ARRAY CONFIGURATIONS

THESIS

Presented to the Faculty of the School of Engineering
of the Air Force Institute of Technology

Air University

In Partial Fulfillment of the
Requirements for the Degree of
Master of Science in Astronautical Engineering

Michael G. Spencer, B.S.

Captain, USAF

December 1988

Approved for public release; distribution unlimited

Table of Contents

	Page
Acknowledgements	ii
List of Figures	v
List of Tables	vi
Abstract	viii
I. Introduction	1
Background	1
Objective	3
Approach	3
II. Orbit Motion Theory	4
Background	4
Development	4
III. Array Antenna Theory	12
Background	12
Antenna Pattern	13
Electric Field Calculation	15
Half-Power Beamwidth	20
IV. Arrays and Program	22
Input	22
Initial Positions	25
Initial Velocities	28
Beamwidth Subroutine	29
Orbit Subroutine	32
V. Results and Analysis	33
Program Check	33
Initial Results	35
Sphere Analysis	46
VI. Conclusions and Recommendations	63
Summary	63
Recommendations	64

Appendix: Computer Program	65
Bibliography	75
Vita	76

List of Figures

Figure	Page
1. Orbital Coordinate Frame	5
2. Two-Element Array of Nondirectional Emitters . .	15
3. Antenna Pattern for Two Emitters	17
4. Three Element Array	17
5. Main Program Flow Chart	23
6. Rectangular Planar Array	26
7. 19 Element, Evenly Spaced Disk Array	26
8. 19 Element Cone Array	27
9. Randomly Spaced Sphere	27
10. Pointing Vector Coordinate System	30
11. Subroutine EFIELD Flow Chart	31
12. Linear Array HPBW Plot	34
13. Rectangular Plane Configurations	37
14. Rectangular Plane HPBW Contours	38
15. Disk Array Configurations	39
16. Disk Array HPBW Contours	40
17. Cone Array Configurations	42
18. Cone Array HPBW Contours	43
19. 20 Emitter Sphere Configurations	44
20. 20 Emitter Sphere HPBW Contours	45
21. Sphere 1 HPBW Contours	48
22. Sphere 2 HPBW Contours	49
23. Random Sphere A HPBW Contours	51
24. Random Sphere B HPBW Contours	52

25.	Random Sphere C HPBW Contours	53
26.	Five Element Sphere HPBW Contours	55
27.	Twenty-five Element Sphere HPBW Contours	56
28.	200 Element Sphere HPBW Contours	57
29.	Early Orbit HPBW Contours for Sphere X	59
30.	Mid-Orbit HPBW Contours for Sphere X	60
31.	Late Orbit HPBW Contours for Sphere X	61
32.	Final HPBW Contour for Sphere X	62

List of Tables

Table		Page
I.	Position Result Comparison	32
II.	Minimum and Maximum HPBW Values	45
III.	Three Random Sphere Beamwidths	48

Abstract

The purpose of this thesis was to develop a computer program to model the motion and radar beam characteristics of different configurations for the distributed sparse array. The effect of the two-body motion on the beam quality of the array was analyzed. Two groups of arrays, planar and three-dimensional were considered. The planar phased arrays were rectangles and disks, and the other arrays included cones and spheres. The number of emitters in the configurations ranged from five to two hundred.

The beam quality parameter was the half-power beamwidth as determined in discrete directions throughout the hemisphere below the array. An array was considered feasible if the beamwidths degraded only slightly during an orbit.

The most useful configuration was found to be a sphere of randomly spaced emitters because it provided narrow beamwidths in all directions below the array. Because of the motion of the array, the beamwidths changed in a predictable, periodic manner. The half-power beamwidths actually improved in certain directions and only slightly degraded in others. The sphere also required the least number of emitters and could be used at any altitude.

EFFECT OF TWO-BODY MOTION ON RADAR BEAM QUALITY FOR VARIOUS
DISTRIBUTED SPARSE ARRAY CONFIGURATIONS

I. Introduction

Background

In 1986 the USAF unveiled a study, Project Forecast II, that established chosen technologies and systems concepts as initiatives for the Air Force Systems Command to pursue and for operational commands to support. The study identified thirty-nine technologies and thirty-one advanced systems concepts which would "revolutionize the way the Air Force carries out its mission in the twenty-first century, ...". A third of the systems concepts listed were related to spacecraft or space missions. This thesis is concerned with the concept of a "distributed sparse array of spacecraft." The idea "involves placing large phased arrays in space with major components of the array not rigidly connected to each other" (2:47,49).

Phased array radars are ideal for search and tracking of targets over large areas because of the ability to electronically steer the radar beam. Hundreds of targets can be tracked almost simultaneously by moving the beam from target to target in a matter of microseconds. An example of

such capabilities is the PAVE PAWS radar system. A single array can span 120 degrees in azimuth and follow a large number of objects almost simultaneously by electronically shifting its beam from one target to another within a few millionths of a second (1:95).

The distributed sparse array radar network could be used for detection and early warning of bomber or cruise missile attacks. Cruise missiles are a threat because they can fly close to the surface under radar beams and around defenses. Look-down sensors, particularly space-based radars provide feasible means of detecting the missiles. The radars could expand the earth coverage for better warning and tracking (3:78).

The distributed sparse array also introduces a new degree of survivability. The network would consist of several nonsophisticated and relatively inexpensive satellites which would reduce the reliance on a few extraordinarily capable, expensive and vulnerable satellites. "It therefore may be possible to create a phased array device that we can place into space and enhance simply by adding more relatively inexpensive elements whenever the threat increases and budget pressures permit" (2:49).

The idea of a large phased array in space is appealing but also very complicated. For a distributed phased array, each element would be in its own orbit and therefore the array would tend to drift apart with time. Placing a large

planar array in space and maintaining the elements to fixed relative positions would require enormous amounts of fuel onboard. A planar array would therefore not be cost effective if employed as a distributed sparse array.

Objective

The objective of this thesis was to analyze possible configurations and determine how the radar beam changed during an array's orbit. The array needed to form a beam with an adequate beamwidth in any direction from the array at any time in the orbit.

Approach

To analyze the effect of the relative motion of the satellites on the beam quality, a computer program was developed. The program used the locations of the emitters, determined the phase differences, and calculated the magnitude of the electric field in a given direction. In incremental angular steps, the field in various directions was evaluated and used to determine the half-power beamwidth (HPBW). The HPBW was then calculated throughout the hemisphere below the array each time the array was moved in its orbit. Plots of the HPBW values were analyzed to find configurations and initial conditions which caused little change in HPBW values during the orbit of the array.

II. Orbit Motion Theory

Background

The configuration of the distributed sparse phased array is a network of several satellites within a region of space. The satellites are in separate orbits and therefore the relative positions to the center of the array will change as the satellites progress around in their orbits. The electric field of the array depends on the relative positions of the emitters. For the array configuration to remain effective, the electric field pattern needs to remain relatively unchanged throughout the orbit.

To determine the effect of the motion, the relative locations of the many satellites at any time in their orbits needed to be calculated. For the relative positions of the array, the motion of the satellites was with respect to the center of the array. The center of the array configuration was assumed to be in a circular orbit. The orbital analysis was based on the Clohessy-Wiltshire equations (10:1).

Development

The motion of the array was developed by first considering its kinematics. The array elements were considered point masses about the central emitter which was assumed to be a point mass in motion in a rotating reference frame fixed to the earth. The vector positions of each

The $\hat{e}_r, \hat{e}_\theta, \hat{e}_z$ axis frame rotates about the earth with the orbital angular velocity $\bar{\omega}^i = \omega \hat{e}_z$.

Taking two time derivatives of equation (2) would give the inertial acceleration of each satellite about the center. Equation (3) was the notation for the absolute rate of change of a rotating system where $(\dot{\bar{r}})_r$ was the rate of change relative to the rotating system (4:48).

$$\dot{\bar{r}} = (\dot{\bar{r}})_r + \bar{\omega} \times \bar{r} \quad (3)$$

The velocity of a satellite was expressed as:

$$\dot{\bar{r}}_2 = (\dot{r} + \delta\dot{r})\hat{e}_r + \dot{r}_0 \delta\theta \hat{e}_\theta + r_0 \delta\dot{\theta} \hat{e}_\theta + \delta z \hat{e}_z + \bar{\omega} \times \bar{r} \quad (4)$$

where $\bar{\omega} \times \bar{r} = \omega(r_0 + \delta r)\hat{e}_\theta - \omega(r_0 \delta\theta)\hat{e}_r$.

By taking another time derivative, the inertial acceleration was expressed as:

$$\ddot{\bar{r}}_2 = (\delta\ddot{r} + \dot{\omega}r_0 \delta\theta - \omega\dot{r}_0 \delta\theta - \omega r_0 \delta\dot{\theta})\hat{e}_r + (\dot{r}\delta\dot{\theta} + r_0 \delta\ddot{\theta} + \dot{\omega}(r_0 + \delta r) + \omega\dot{r}_0 + \omega\delta\dot{r})\hat{e}_\theta + \delta z \hat{e}_z + \bar{\omega} \times \dot{\bar{r}} \quad (5)$$

where

$$\bar{\omega} \times \dot{\bar{r}} = \omega(\delta\dot{r} - \omega r_0 \delta\theta)\hat{e}_\theta - \omega[r_0 \delta\dot{\theta} + \omega(r_0 + \delta r)]\hat{e}_r$$

For satellites in two-body, circular orbits, the angular and radial velocities were constant.

Therefore:

$$\dot{\omega} = 0 \quad \text{and} \quad \dot{r}_0 = 0$$

The mean orbit period was $P = 2\pi(a^3/\mu)^{1/2}$

The angular velocity ω is the rate the central satellite completes an orbit. Because $\omega = \frac{2\pi}{P}$, the angular velocity equals the mean motion ($\omega = n$). These relations reduced equation (5) to

$$\begin{aligned} \ddot{\bar{r}}_2 = & [\delta\ddot{r} - 2nr_0\delta\dot{\theta} - n^2(r_0 + \delta r)]\hat{e}_r \\ & + [r_0\delta\ddot{\theta} + 2n\delta\dot{r} - n^2r_0\delta\theta]\hat{e}_\theta + \delta\ddot{z}e_z \end{aligned} \quad (6)$$

Assuming the array was in a two-body orbit then equation (7) expresses the gravitational acceleration (10:2).

$$\bar{a}_g = \frac{-\mu\bar{r}}{r^3} \quad (7)$$

The magnitude of $\bar{r}_2 = \bar{r}_0 + \bar{\rho}$ was:

$$r_2 = (r_0^2 + 2\bar{r}_0 \cdot \bar{\rho} + \rho^2)^{1/2}$$

Therefore,

$$r_2^{-3} = \left\{ r_0^2 \left[1 + \frac{2\bar{r}_0 \cdot \bar{\rho}}{r_0^2} + \left(\frac{\rho}{r_0} \right)^2 \right] \right\}^{-3/2} \quad (8)$$

From equation (8), ϵ was defined as $\epsilon = \frac{2\bar{r}_0 \cdot \bar{\rho}}{r_0^2} + \left(\frac{\rho}{r_0} \right)^2$

The term $(1+\epsilon)^{-3/2}$ was expanded with the binomial expansion. Keeping first order terms of $\bar{\rho}$ yielded:

$$r_2^{-3} \approx r_0^{-3} \left[1 - \frac{3}{2}\epsilon \right] = r_0^{-3} \left[1 - 3 \left(\bar{r}_0 \cdot \frac{\bar{\rho}}{r_0^2} \right) \right] \quad (9)$$

Now r_2 was put in terms of the $\hat{e}_r, \hat{e}_\theta, \hat{e}_z$ coordinate system,

$$r_2^{-3} = (r_0^2 + 2r_0\delta r + \delta r^2 + r_0^2\delta\theta^2 + \delta z^2)^{-3/2} \quad (10)$$

The δr , $\delta\theta$, and δz were small with respect to r_0 so that δr^2 , $\delta\theta^2$, and δz^2 were approximately equal to zero.

Equation (10) was rewritten as:

$$r_2^{-3} \approx r_0^{-3} (1 + \epsilon)^{-3/2} \quad \text{where } \epsilon \approx \frac{2\delta r}{r_0} \quad (11)$$

By using the binomial expansion as before, equation (11) was reduced to:

$$r_2^{-3} \approx r_0^{-3} (1 - 3\delta r/r_0) \quad (12)$$

This expression for r_2^{-3} was used in the denominator of equation (7) to give:

$$\bar{a}_g = \frac{-\mu}{r_0^3} \left[(r_0 + \delta r)\hat{e}_r + r_0\delta\theta\hat{e}_\theta + \delta z\hat{e}_z \right] \left[1 - 3\delta r/r_0 \right] \quad (13)$$

The squares of the δ terms were ≈ 0 , and for a circular orbit:

$$a = r_0 \quad \text{and} \quad n = \left(\frac{\mu}{r_0^3} \right)^{1/2}$$

Equation (13) was then simplified to:

$$\bar{a}_g \approx -n^2 \left[(r_0 - 2\delta r)\hat{e}_r + r_0\delta\theta\hat{e}_\theta + \delta z\hat{e}_z \right] \quad (14)$$

Assuming the array underwent only two-body motion, then the gravitational acceleration and the kinematic accelerations were equal.

Setting $\ddot{\bar{a}}_g = \ddot{\bar{r}}$ gave:

$$(\delta\ddot{r} - 2nr_0\delta\dot{\theta} - 3n^2\delta r)\hat{e}_r + (r_0\delta\ddot{\theta} + 2n\delta r)\hat{e}_\theta + (\delta\ddot{z} + n^2\delta z)\hat{e}_z = 0 \quad (15)$$

Equation (15) shows the motion in the \hat{e}_z direction is uncoupled from the \hat{e}_r , and \hat{e}_θ directions. The solution for the δz displacement was found to be a simple harmonic oscillator. The initial conditions when $t = 0$ were:

$$\delta z(0) = \delta z_0 \quad \text{and} \quad \delta\dot{z}(0) = \delta\dot{z}_0$$

Therefore,

$$\delta z(t) = \delta z_0 \cos(nt) + \frac{\delta\dot{z}_0}{n} \sin(nt) \quad (16)$$

$$\delta\dot{z}(t) = -n\delta z_0 \sin(nt) + \delta\dot{z}_0 \cos(nt) \quad (17)$$

The \hat{e}_θ components were integrated with the initial conditions of $\delta\theta(0) = \delta\theta_0$ and $\delta\dot{\theta}(0) = \delta\dot{\theta}_0$ to give:

$$r_0\delta\dot{\theta}(t) = 2n(\delta r_0 - \delta r(t)) + r_0\delta\dot{\theta}_0 \quad (18)$$

Equation (18) was used in the \hat{e}_r component to give

$$\delta\ddot{r} - 4n^2\delta r_0 + n^2\delta r - 2nr_0\delta\dot{\theta}_0 = 0 \quad (19)$$

With the initial conditions, $\delta r(0) = \delta r_0$ and $\delta\dot{r}(0) = \delta\dot{r}_0$ the homogeneous and particular solutions were:

$$\delta r(t)|_h = A \cdot \cos(nt) + B \cdot \sin(nt) \quad (20a)$$

$$\delta r(t)|_p = 4\delta r_0 + \left(\frac{r_0}{n}\right)\delta\dot{\theta}_0 \quad (20b)$$

The complete solution for the \hat{e}_r direction was then

$$\delta r(t) = \left(-3\delta r_0 - \frac{2}{n}(r_0 \delta \dot{\theta}_0)\right) \cos(nt) + \frac{\delta \dot{r}_0}{n} \sin(nt) + 4\delta r_0 + \frac{2}{n} r_0 \delta \dot{\theta}_0 \quad (21)$$

$$\delta \dot{r}(t) = (3n\delta r_0 + 2r_0 \delta \dot{\theta}_0) \sin(nt) + \delta \dot{r}_0 \cos(nt) \quad (22)$$

Using the solution for $\delta r(t)$ in equation (18) gave the solution for $r_0 \delta \dot{\theta}(t)$:

$$r_0 \delta \dot{\theta}(t) = -3r_0 \delta \dot{\theta}_0 - 6nr_0 \delta r_0 + \left(6n\delta r_0 + 4r_0 \delta \dot{\theta}_0\right) \cos(nt) - (2\delta \dot{r}_0) \sin(nt) \quad (23)$$

Integrating equation (23) gave the solution for $r_0 \delta \theta(t)$.

$$r_0 \delta \theta(t) = r_0 \delta \theta_0 - \left(3r_0 \delta \dot{\theta}_0 + 6n\delta r_0\right) t + \left(6n\delta r_0 + \frac{4}{n} r_0 \delta \dot{\theta}_0\right) \sin(nt) + \left(\frac{2\delta \dot{r}_0}{n}\right) \cos(nt) - \frac{2\delta r_0}{n} \quad (24)$$

Equations 16, 17 and 21 - 24 represent the equations of motion in the \hat{e}_r , \hat{e}_θ , and \hat{e}_z coordinate system for a satellite in an orbit near the center of the array. For use with several satellites the equations were written in matrix form in equation (25) (10:2-6).

$$\delta R_i(t) = \begin{Bmatrix} \delta r(t) \\ r_o \delta \theta(t) \\ \delta z(t) \end{Bmatrix} \quad \text{and} \quad \delta V_i(t) = \begin{Bmatrix} \delta \dot{r}(t) \\ r_o \delta \dot{\theta}(t) \\ \delta \dot{z}(t) \end{Bmatrix} \quad (25)$$

$$\delta R_i(t) = \Phi_{rr} \delta \bar{r}(t=0) + \Phi_{rv} \delta \bar{v}(t=0) \quad (26a)$$

$$\delta V_i(t) = \Phi_{vr} \delta \bar{r}(t=0) + \Phi_{vv} \delta \bar{v}(t=0) \quad (26b)$$

The Φ_{xx} matrices were defined in equations (27a-d) where $\Psi = nt$, and t was in seconds (10:6).

$$\Phi_{rr} = \begin{bmatrix} (4-3\cos\Psi) & 0 & 0 \\ 6(\sin\Psi - \Psi) & 1 & 0 \\ 0 & 0 & \cos\Psi \end{bmatrix} \quad (27a)$$

$$\Phi_{rv} = \begin{bmatrix} 1/n(\sin\Psi) & 2/n(1 - \cos\Psi) & 0 \\ 2/n(\cos\Psi - 1) & 1/n(4\sin\Psi - 3\Psi) & 0 \\ 0 & 0 & 1/n\sin\Psi \end{bmatrix} \quad (27b)$$

$$\Phi_{vr} = \begin{bmatrix} 3n(\sin\Psi) & 0 & 0 \\ 6n(\cos\Psi - 1) & 0 & 0 \\ 0 & 0 & -n(\sin\Psi) \end{bmatrix} \quad (27c)$$

$$\Phi_{vv} = \begin{bmatrix} \cos\Psi & 2\sin\Psi & 0 \\ -2(\sin\Psi) & -3 + 4\cos\Psi & 0 \\ 0 & 0 & \cos\Psi \end{bmatrix} \quad (27d)$$

The only variables in these equations were the initial positions and velocities, orbit altitude and amount of time the array moved. Knowing these parameters, the matrices $\delta R_i(t)$ and $\delta V_i(t)$ gave the displacements in the \hat{e}_r , \hat{e}_θ , and \hat{e}_z directions after the satellites had moved t seconds.

III. Array Antenna Theory

Background

Phased array radars are ideal for search and tracking of targets over large areas because of the ability to electronically steer the radar beam. Hundreds of targets can be tracked almost simultaneously by moving the beam from target to target in a matter of microseconds. A phased array radar works by a group of identical emitters each radiating its energy from the array. Depending on the shape of the antenna, the radiation forms a narrow, pencil-like beam, suited for tracking or a fan-like beam, best for searching broad areas (1:94).

When all the signals leave the array in phase, they will add in phase at any point along a line perpendicular to the plane of the array. The signals constructively interfere (add) along the array's boresight, or perpendicular axis, and within a small angle to each side. At greater angles to the boresight, individual signals from different radiating elements must travel different distances to reach a target. As a result the relative phases are changed and the signals interfere destructively. Thus, outside the narrow cone, centered on the array's boresight, targets produce no detectable return. Because of the characteristics of interference patterns, the width of that

cone is directly proportional to the operating wavelength and inversely proportional to the size of the array (1:96)

Beam steering is accomplished when the signals from each of the radiating elements are delayed electronically by amounts that increase steadily across the array. Each delay causes a signal to lag a fraction of a wavelength behind the signal from the adjacent element. The zone in which the signals add up in phase to produce a return signal lies not down the boresight of the antenna, but off to the side in the direction of increasing phase delay. The angle of the beam reflects the magnitude of the phase shift, the size of the array and the wavelength of the signals. The beam has the form of a slender cone surrounded by regions of destructive interference (1:96).

Antenna Pattern

The distributed sparse array network is a general form of a phased array radar. To determine the beam characteristics of a phased array radar, the radiation patterns from all the emitters are combined to give the overall antenna pattern. The antenna pattern is then used to show the direction and relative magnitude of the emitted power. The antenna pattern depends on the orientations, positions in space, amplitudes and phasing of the emitters. (9:109)

The radiation pattern also depends on the distance from the antenna that the field is measured. If the pattern is measured sufficiently far from the antenna for there to be no change in pattern with distance, the pattern is the far-field pattern. Measurements at lesser distances yield near-field patterns, which are a function of both angle and distance. The pattern may be expressed in terms of the electric field intensity (field pattern) or in terms of the radiation intensity (power patterns) (6:604).

The pattern usually has many lobes. The main lobe is the lobe containing the direction of maximum radiation. Any lobe other than the main lobe is called a minor or side lobe. Typically the side lobes are alternately positive and negative valued. A pattern in its most general form may be complex-valued. In that case, the magnitude of the electric field pattern $|E(\theta)|$ or the power pattern $P(\theta)$ is used to generate the antenna pattern (9:29).

With antennas such as dipoles and horns, the radiation pattern is usually expressed in terms of the power density (power patterns). Analyzing array antennas, however, involves the addition of the field contributions from the entire array. The antenna pattern is then based on the field pattern because the magnitudes and phases of the elements must be considered (6:627).

Electric Field Calculation

For most phased-array radars the antenna pattern is developed by making certain geometric constraints such as a planar array with evenly spaced emitters. This approach was not used in this case because the sparse 3-dimensional geometry of the array did not lead to such simplifications. However, the analysis for the sparse array was accomplished in a similar manner as with an n element array. The method is developed with the following examples.

The emitters were assumed to be isotropic point source radiators with the same amplitude as the reference source. In the first example, two identical point source radiators were spaced a distance d apart. In Figure 2 the field was determined at a point p , far from the emitters (5:398).

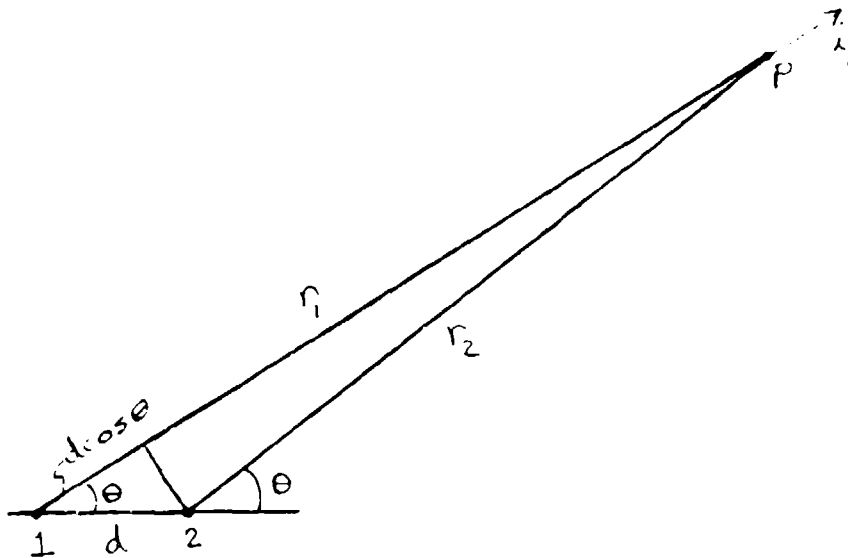


Figure 2. Two-Element Array of Nondirectional Emitters

Because the point p was very far from the emitters, the distance r_1 was approximated by

$$r_1 = r_2 + d \cos \theta \quad (28)$$

The sum of the electric fields at p was

$$E_T = E_1 + E_2 e^{j\psi} \quad (29)$$

where

$$\psi = \beta d \cos \theta + \alpha$$

$$\beta = 2\pi / \lambda$$

$$\alpha = \text{progressive phase shift}$$

$$d \cos \theta = \text{path difference}$$

The progressive phase shift is used to electronically steer the antenna main beam. For linear arrays, adding a constant phase to each emitter will point the beam into the new direction of interest. For the two identical emitters the broadside beam pattern is obtained when $\alpha = 0$.

Therefore,

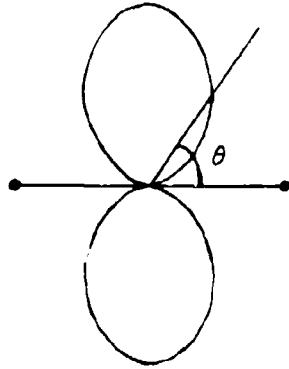
$$E_T = E_1 | (1 + e^{j\psi}) | \quad (30)$$

$$= E_1 \sqrt{(1 + \cos \psi)^2 + \sin^2 \psi} \quad (31)$$

$$= 2E_1 \cos (\psi / 2) \quad (32)$$

The field pattern only depends on the distance between the two emitters, d , and the direction θ . When $d = \lambda/2$, then $\psi = \pi \cos \theta$ and the field pattern is shown in Figure 3.

The next example used three emitters in a plane but not linearly spaced. Figure 4 shows the three emitters spaced distances d_2 and d_3 apart (5:400).



$$d = \lambda/2 \text{ and } \alpha = 0$$

Figure 3. Antenna Pattern for Two Emitters

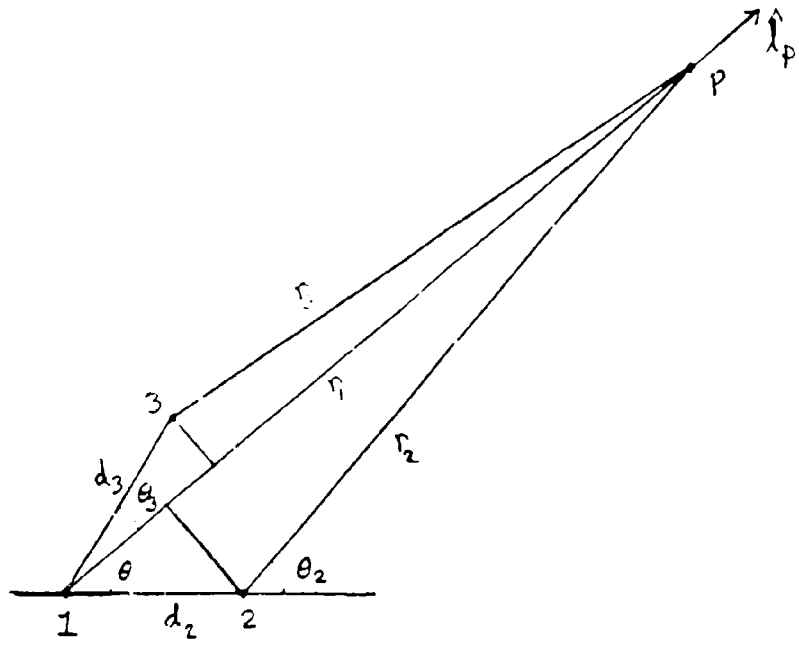


Figure 4. Three Element Array

The electric field was again measured at point p, far from the array such that the distances r_2 and r_3 were approximated by

$$r_2 = r_1 - d_2 \cos \theta_2 \quad r_3 = r_1 - d_3 \cos \theta_3$$

When emitter 1 was the reference emitter, the total electric field was the sum:

$$E_T = E_1 + E_2 e^{j\psi_2} + E_3 e^{j\psi_3} \quad (33)$$

where

$$\psi_1 = \beta d_1 \cos \theta_1 + \alpha_1$$

ψ_1 = the phase difference

$$\beta = 2\pi / \lambda$$

α_1 = the progressive phase shift

If all the emitters are identical the total electric field is written as:

$$E_T = E_1 (1 + e^{j\psi_2} + e^{j\psi_3}) \quad (34)$$

The antenna pattern would be a graph of the magnitude of the electric field

$$E_T = E_1 |(1 + e^{j\psi_2} + e^{j\psi_3})| \quad (35)$$

Because the positions of the emitters were not linear or symmetrical, the phase differences could not be simplified into a single function as was the case for the two point emitters. To determine the magnitude of E_T , the exponent terms were recast into real and imaginary parts. The magnitude is given by the square root of the sum of the squares of the real and imaginary parts.

$$E_T = E_1 \left[(1 + \cos\psi_2 + \cos\psi_3)^2 + (\sin\psi_2 + \sin\psi_3)^2 \right]^{1/2} \quad (36)$$

This method made use of the principle of superposition, and can be generalized into three dimensions with any number of emitters; i.e., the total field was the sum of the fields due to each component. From each emitter the phase difference depended on two parts: 1) the path difference, and 2) the phase shift. For isotropic point source emitters, the amplitude could vary so that in general, the total electric field was the sum over all emitters as given by equation (37) (8:99-106).

$$E_T = \sum_i E_i = \sum_i A_i \exp[j\beta(\Delta_i) + j\psi_i] \quad (37)$$

where

A_i = amplitude of each emitter

Δ_i = path difference of each emitter to the point p

ψ_i = phase shift added to point the beam

The path difference was the difference between the position vectors to the emitters and the pointing vector from the reference emitter, \hat{l}_p . This difference was determined by the projection of the position vector to each emitter onto the pointing vector, $(\vec{r}_i \cdot \hat{l}_p)$.

The maximum electric field in any direction occurs when the phase difference is equal to zero. From equation (37), this occurs when:

$$\beta\Delta_i = -\psi_i \quad (38)$$

To point a beam maximum in a given direction \hat{l}_p , the phase shift is calculated from:

$$\beta(\bar{r}_i \cdot \hat{l}_p) = -\psi_i \quad (39)$$

The direction the beam was pointed is defined as \hat{l}_o and rearranging equation (39) gives:

$$\psi_i = -\beta(\bar{r}_i \cdot \hat{l}_o) \quad (40)$$

To evaluate the electric field anywhere else with the main lobe still pointed along \hat{l}_o , the pointing vector, \hat{l}_p , only needs to be moved. Equation (37) can be rewritten as:

$$E_r = \sum_i A_i \exp[j\beta(\bar{r}_i \cdot \hat{l}_p - \bar{r}_i \cdot \hat{l}_o)] \quad (41)$$

Half-Power Beamwidth

A parameter to describe how the power in a direction is emitted is the half-power beamwidth (HPBW). It is the angular separation of the points in the main beam where the power pattern equals one-half of the maximum power. Because the power is related to the square of the electric field, these points correspond to the value $1/\sqrt{2}$ for the field pattern $|E(\theta)|$. The smaller the HPBW angle, the more concentrated the radar energy along the boresight direction.

(9:30)

To calculate the half-power point of the beam, the magnitude of the field in a direction \hat{l}_p was compared to the maximum field strength which was along the boresight

direction, \hat{l}_0 . The half-power point in one direction from the boresight direction was found when the ratio of these magnitudes was given by:

$$\frac{|E_T(l_p)|}{|E_T(l_0)|} = 0.70710678 \quad (42)$$

The half-power beamwidth angle (HPBW) was determined by first assuming the beam was symmetrical about the boresight. The pointing vector was incrementally moved through a plane from the boresight. The electric field was evaluated at each step until the half-power point (equation 47) was found. The HPBW was calculated as double the size of the angle to the half-power point.

IV. Arrays And Program

To analyze the effect of the relative motion of the satellites on the beam quality a computer program was developed. The program used the locations and characteristics of the emitters, determined the phase differences and calculated the magnitude of the electric field in a given direction. Then by incremental angular steps the field in other directions was evaluated and used to determine the half-power beamwidth. The HPBW was then calculated throughout the hemisphere below the array each time the array was moved t seconds. Figure 5 shows the flow chart and the program is listed in the Appendix.

Input

The first input parameter about the arrays which varied was the number of emitters in each array. The program was developed to put up to 240 satellites in an array. Arrays with from 5 to 200 satellites were modeled to determine the effect of the density of emitters. The altitude was another variable to be given in the input. Because many different operating altitudes had been possible, the altitude range considered was from 500 km to geosynchronous orbit.

Other input parameters were related to the emitters. They were all assumed to be identical point source radiators. When calculating the electric field, since all

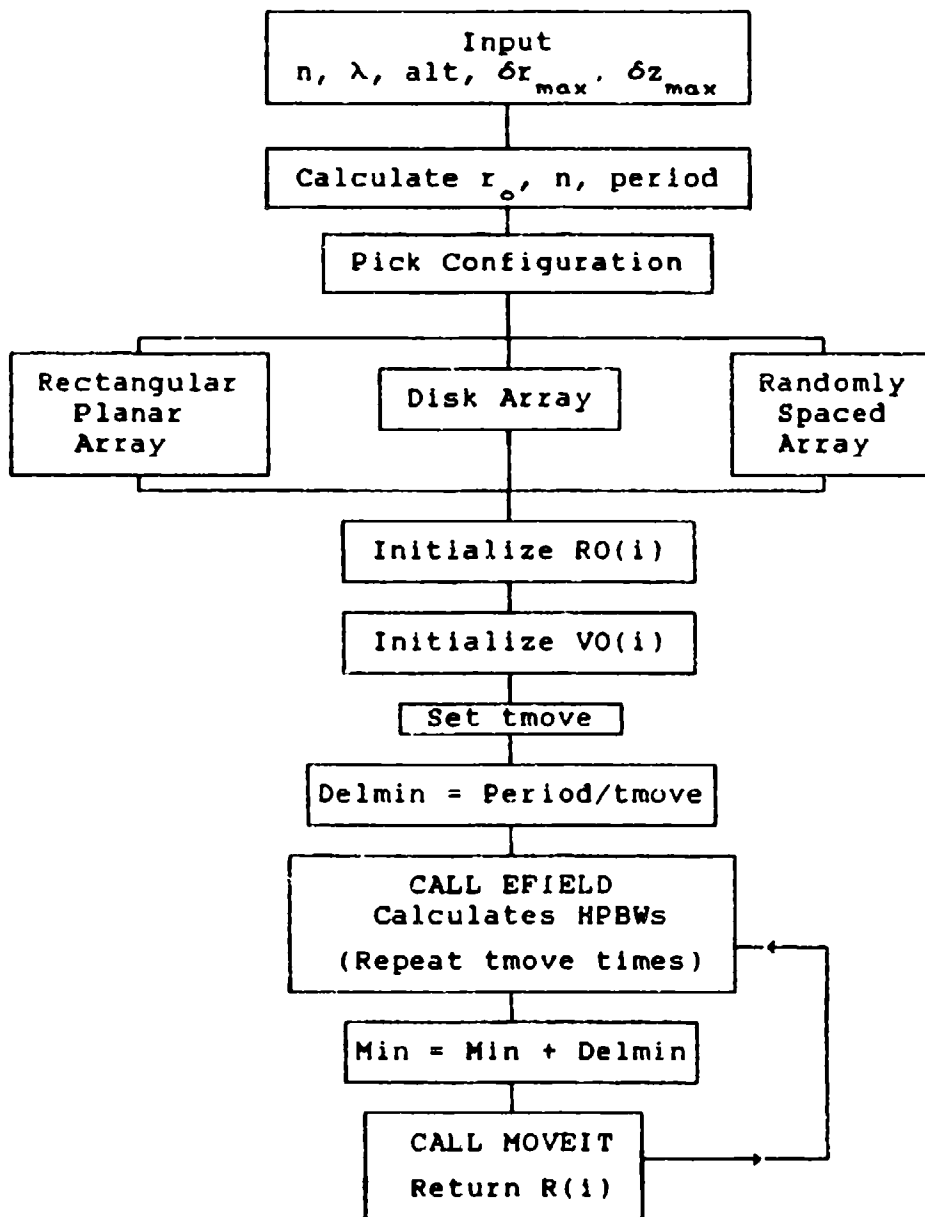


Figure 5. Main Program Flow Chart

the emitters were the same, the amplitudes would factor out. For n emitters, the total electric field would be:

$$E_T = nA_i \sum_i \exp(j\beta\psi_i) \quad (43)$$

where

ψ_i = phase difference for each emitter

$$\beta = 2\pi/\lambda$$

Because the HPBW is determined from the ratio of the electric field in the desired direction versus the field along the boresight of the beam, the amplitudes of the emitters will cancel. Therefore, as long as the emitters are identical, the amplitudes can be arbitrary and for the program they were assumed to be equal to one.

The wavelength of the radiated signal is another input parameter. The magnitude of the electric field is directly proportional to the dimensions of the array and inversely proportional to the wavelength (r_i/λ). The units of r_i and λ therefore, must be same. In the program,

$$\mu = 3.986012 \text{ km}^3/\text{s}^2 \quad (44)$$

For the mean motion, ($n = \sqrt{\mu/r}$), to have the correct units of seconds, the radial distance r_0 and the displacements δr , $r_0 \delta\theta$, and δz were assumed to have the units of kilometers. To keep the units correct and to normalize the dimensions, the wavelength was assumed to be one kilometer. The actual dimensions of the array were not of interest, only the relative beamwidth changes. The wavelength was therefore a scale factor for the relative positions.

Initial Positions

The next part of the program involved the input for the positions of the array. The most common phased array radars are planar arrays made up of hundreds to thousands of elements. The arrays are usually fixed to a building or platforms and radiate for specific areas of coverage. Locating the array in space provides the opportunity to put the array into a three-dimensional configuration. The different types of array configurations considered for this project included two and three-dimensional arrays.

For the rectangular planar arrays, the x and y coordinates of the emitters were the input data. A scale factor to increase or shrink the overall size of the array and a tilt angle to rotate the array about the \hat{e}_θ axis were also given as input.

The next type of planar arrays were called disks. These configurations involved placing elliptical or spherical rings of varying numbers of emitters around the center. The shape of the ring could be modified by changing the eccentricity of the ring. Cone arrays were made by placing emitters at different radial altitudes.

The final shapes were spheres of randomly spaced emitters. The input was the lengths of the sphere in each direction. A random number generating routine calculated the e_r , e_θ , and e_z displacements. Example configurations are shown in Figures 6 - 9.

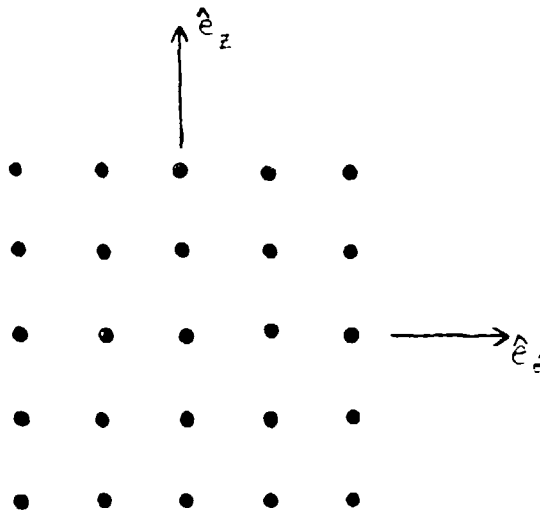


Figure 6. Rectangular Planar Array

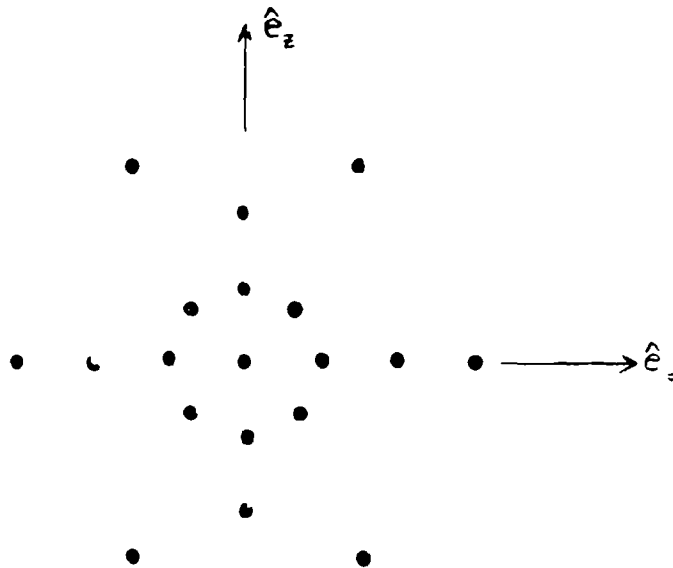


Figure 7. 19 Element, Evenly Spaced Disk Array

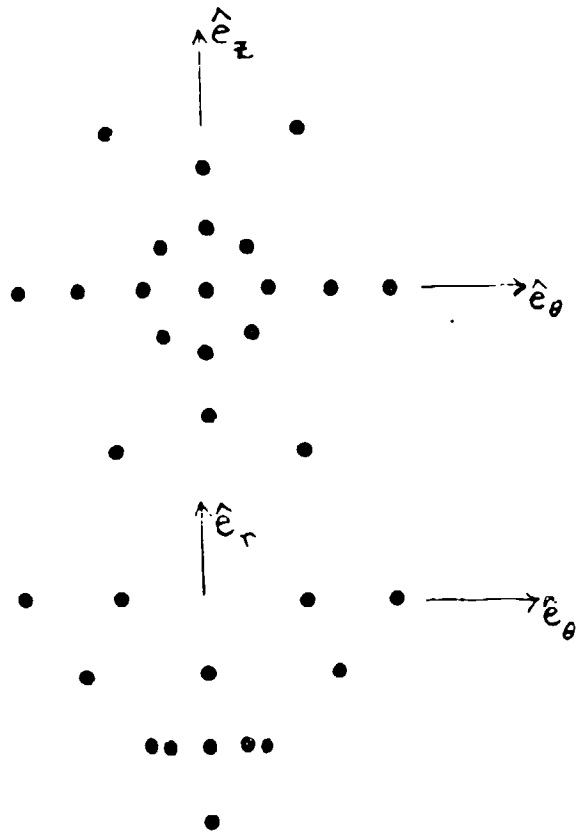


Figure 8. 19 Element Cone Array

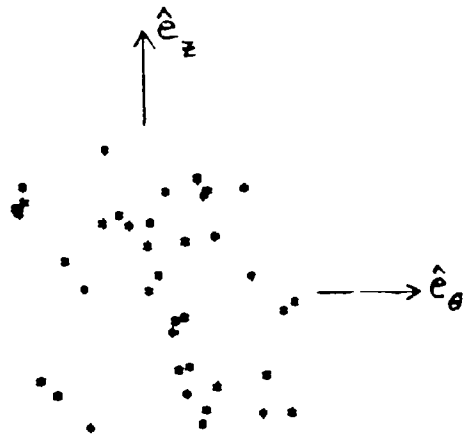


Figure 9. Randomly Spaced Sphere

Initial Velocities

Once the initial positions were given for any particular array, the only remaining information to obtain was the initial velocity conditions. Although the satellites will not remain in a fixed orientation with respect to the reference satellite, under certain initial conditions the motion could be confined to a specified region of space. In equations (16) and (21), the radial and vertical displacements have constant and time periodic terms. The tangential displacement equation (24) also has constant and periodic terms, but there is also a secular component. To keep the array from forever spreading apart in the \hat{e}_θ direction, the secular component must be made to equal zero. From equation (24),

$$(3r_0\delta\dot{\theta}_0 + 6n\delta r_0) = 0 \quad (45)$$

Solving for the initial tangential velocity:

$$r_0\delta\dot{\theta}_0 = -2n\delta r_0 \quad (46)$$

The tangential initial velocity therefore depends on the initial radial displacement. By assuming the only secular velocity term equals zero, the motion of the array is restricted to periodic changes with the period of one orbit. The array will spread apart a maximum distance in one-half of an orbit and then return to the initial positions by the completion of one orbit. When the conditions in equation (46) are set, then the radial displacement becomes an oscillating function.

$$\delta r(t) = [-3\delta r_0 - \frac{2}{n}(r_0 \delta \dot{\theta}_0)] \cos(nt) + \frac{\delta \dot{r}_0}{n} \sin(nt) \quad (47)$$

Equations (16) and (47) were used to develop the relationship between the maximum displacements and the initial velocity components. The initial conditions when $t = 0$ were:

$$\delta r(0) = \delta r_0 \quad \text{and} \quad \delta \dot{r}(0) = \delta \dot{r}_0 \quad (48a,b)$$

$$\delta z(0) = \delta z_0 \quad \text{and} \quad \delta \dot{z}(0) = \delta \dot{z}_0 \quad (49a,b)$$

The $\delta \dot{r}_0$ and $\delta \dot{z}_0$ are values to be determined.

The maximum displacements occur after half an orbit which is when $\psi = \pi/2$. From equations (16) and (47), the maximum displacements were:

$$\delta r(\pi/2) = \frac{\delta \dot{r}_0}{n} \quad \text{and} \quad \delta z(\pi/2) = \frac{\delta \dot{z}_0}{n} \quad (50)$$

The initial velocities were then found in terms of a given maximum allowable displacement in each direction.

$$\delta \dot{r}_0 = n\delta r_{\max} \quad \delta \dot{z}_0 = n\delta z_{\max} \quad (51)$$

In the program δr_{\max} and δz_{\max} were set equal to one for the basic analysis.

Beamwidth Subroutine

The subroutine EFIELD was used to evaluate the electric field by incremental steps in the hemisphere below the array. The magnitudes of the electric fields were used to determine the HPBW angle. The routine used the locations of the emitters to calculate the phase difference for each direction. The coordinate system used to determine the look

directions and phase differences is shown in Figure 10. The angle ϕ ranged from 0° to 90° while the angle θ ranged from 0° to 360° . The angular steps were 15° in both directions. Fifteen degrees was chosen because it provided enough change when calculating the field without creating too much data for the plotting program.

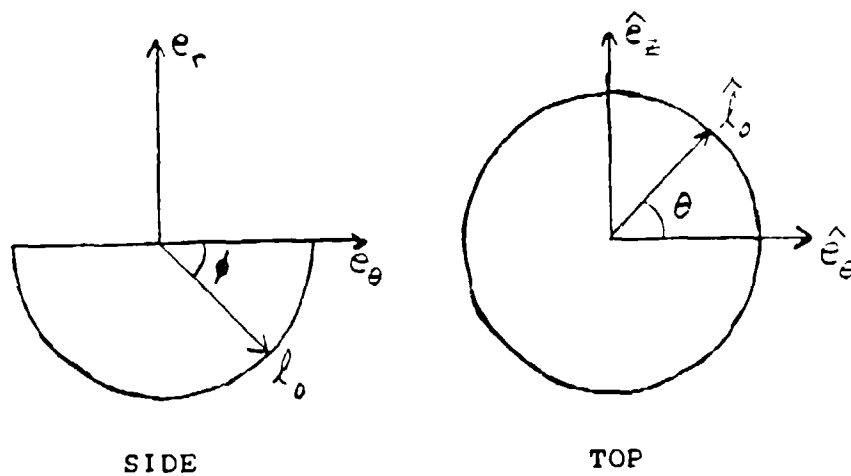


Figure 10. Pointing Vector Coordinate System

To determine the half-power point, the point direction, \hat{l}_p was changed in the ϕ direction. The field in that direction was compared to the beam maximum field value until the half-power point was found. The algorithm used a step-down process to locate the bounds for a bisection search which determined the half-power point. The beam was assumed to be symmetrical about the boresight so that the half-power beamwidth was twice the angle to the half-power point. The flow chart for the subroutine EFIELD is shown in Figure 11.

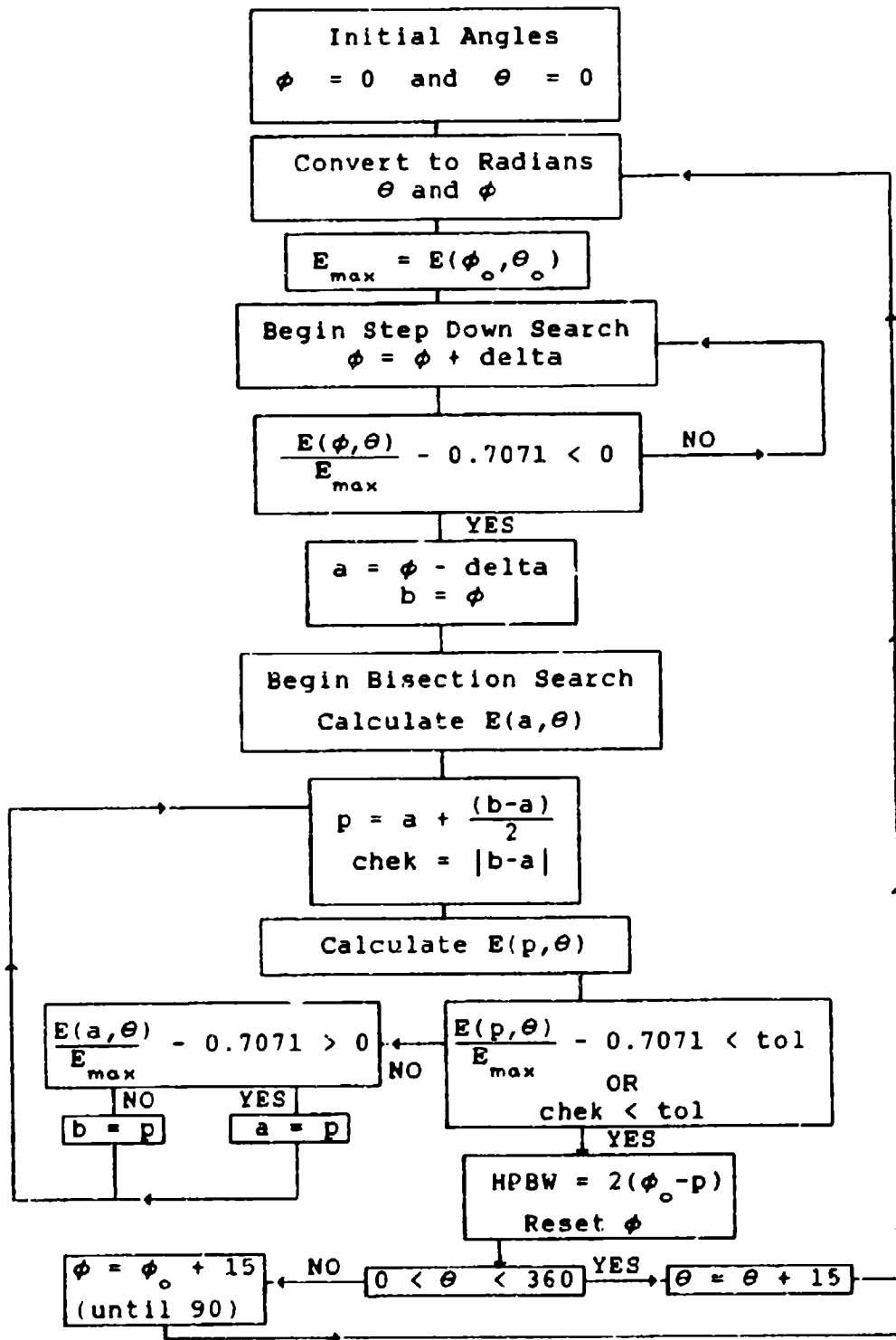


Figure 11. Subroutine EFIELD Flow Chart

Orbit Subroutine

Once the half-power beamwidths in all directions were calculated and recorded, the next step was to move the array forward in time with the subroutine MOVEIT. The amount of minutes to move was determined in the main program and then converted to seconds in the subroutine. Time was made dimensionless by $\psi = n \times t$. The Φ_{xx} matrices, equations (27a-d), were evaluated and used to calculate $\delta R_i(t)$ and $\delta V_i(t)$. The new positions $\delta R_i(t)$ were then returned to the main program for the half-power beamwidths to be recalculated.

V. Results And Analysis

Program Check

To test the validity of the program, a linear array of 20 emitters was used with a spacing of $\lambda/2$. The values for the HPBW were computed and compared to the known solutions in reference 6. The HPBWs in the \hat{e}_θ plane are shown in Figure 12. The pattern is shown only in the plane of the array because the field of the linear array is symmetric about the axis of the array. The actual three dimensional antenna pattern is a disk shaped figure obtained by rotating the pattern about the \hat{e}_θ axis (6:635).

The calculated broadside and endfire HPBWs were 5.08° and 34.25° . The text values were 5.1° and 34° . As Figure 12 shows, the HPBW increased as the beam was pointed towards the endfire direction (6:635).

To check the motion subroutine, a random sphere with three elements was used. The initial positions were generated by the program. With these positions and δr_{\max} and δz_{\max} equal to one, the initial velocities, n , and the period were calculated. The positions at different points in the orbit were calculated with a hand calculator. These values and the program results for one point are listed in Table I. The program gave the same results.

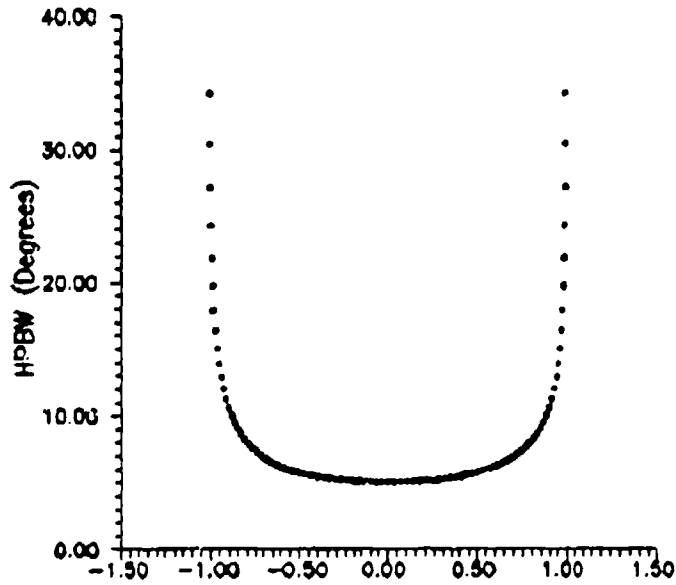


Figure 12. Linear Array HPBW Plot

Table I. Position Result Comparison

Method	ψ	δr	$r_0 \delta \theta$	δz
Program	0	-91.7001	37.1940	31.2645
	$\pi/3$	46.7161	193.0233	-14.7662
	2π	-91.7001	37.1941	31.2645
Calculat.	0	-91.7001	37.1940	31.2645
	$\pi/3$	46.7157	192.1637	-14.7662
	2π	-91.7001	37.1933	31.2645

Initial Results

Overview Each array was evaluated at its initial positions and then after each time it was moved. Before and after configuration and HPBW plots were made for each array. The dimensions on both axes of the configuration plots are in terms of wavelengths. The figures show the relative displacements between the emitters. All displacements were normalized by setting the wavelengths equal to one. The configuration figures show top views of the arrays.

After the half-power beamwidth was calculated, the angles ϕ and θ were converted to rectangular x and y coordinates in the $\hat{e}_\theta - \hat{e}_z$ plane. The positive z axis value was the HPBW value from the ϕ, θ direction below the array. To graph the data, the file of x, y, z data was then used with the SURFER graphics package to generate contour plots. When making the plots, most default settings in the SURFER programs were used.

In the initial analysis, the arrays were only moved $1/3$ of an orbit. The one third orbit point was chosen to avoid the possibility of masking changes in the HPBW caused by symmetric motion that might have occurred at the $1/4$ or $1/2$ orbit points. The $1/3$ orbit point was also chosen to give enough time for a significant change to occur.

Four general types of arrays were developed for the initial analysis. The arrays were 1) a rectangular plane, 2) a disk, 3) a cone and 4) a sphere. These arrays were

evaluated to determine the most feasible configuration for a distributed array. One type of array was chosen and then modified to determine the effects of changing the initial conditions.

Planar Array A twenty-five element, evenly spaced, planar array was the first configuration. The top view of the relative positions before and after moving 1/3 an orbit are shown in Figure 13. Figure 14 shows the HPBW contours before and after 1/3 an orbit. As with the linear array, the HPBW is good near broadside and degrades towards the sides of the array. Planar arrays have limited usable directions because the beam width increases when pointing the beam in the endfire direction.

Disk Array Another form of a planar array was a 19 element, slightly elliptical, disk array. The emitters were evenly spaced in rings about the center. Figure 15 shows the relative positions of the configuration. The motion of this and the rectangular plane are similar because they were both initially in a flat plane with no \hat{e}_x displacements. As these arrays orbit, the dominant oscillating motion was in the \hat{e}_z direction. The motion in the \hat{e}_θ direction was considerably smaller than the initial displacements and cannot be seen on these figures because of the scale. Figure 16 shows the HPBW contours. The results are similar to the rectangular planar array in that the beam width increases towards the endfire conditions.

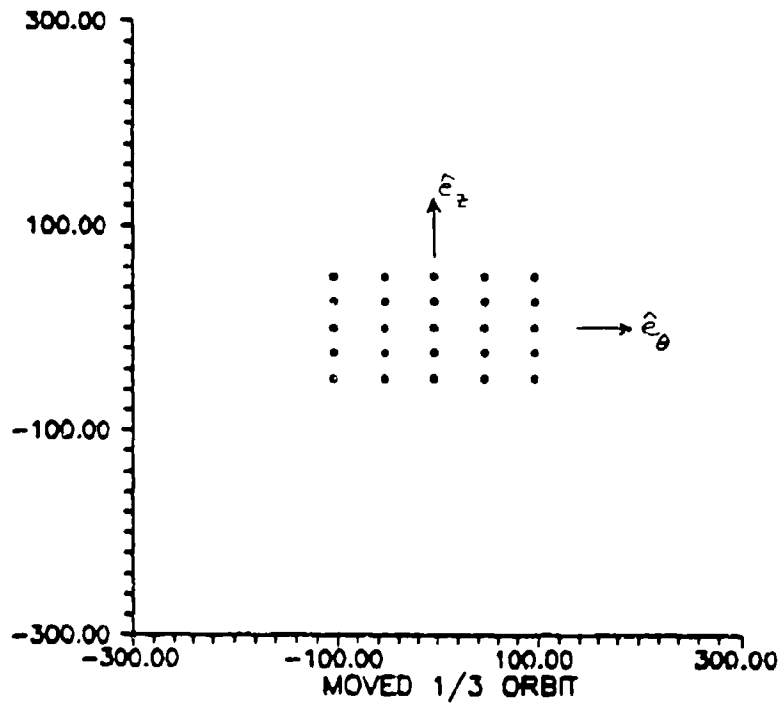
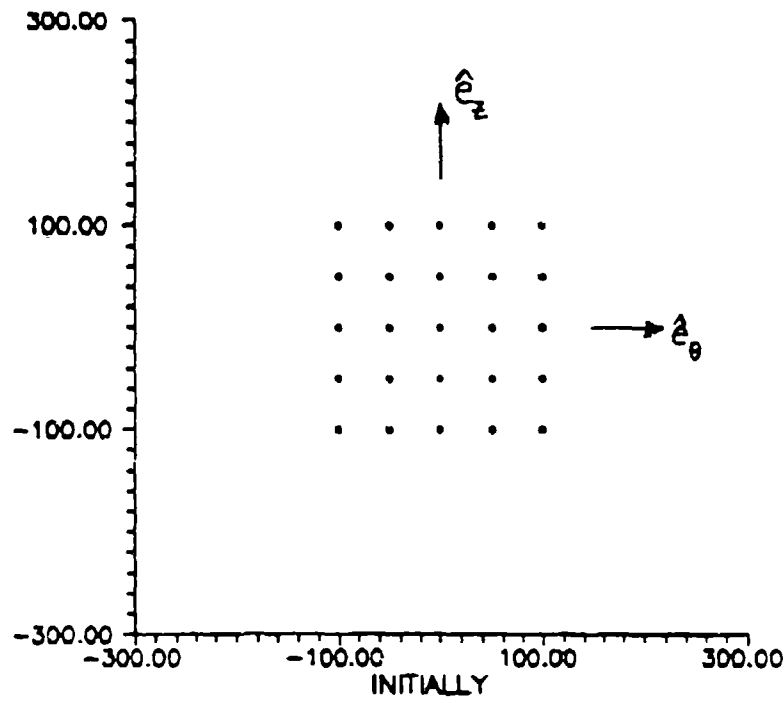
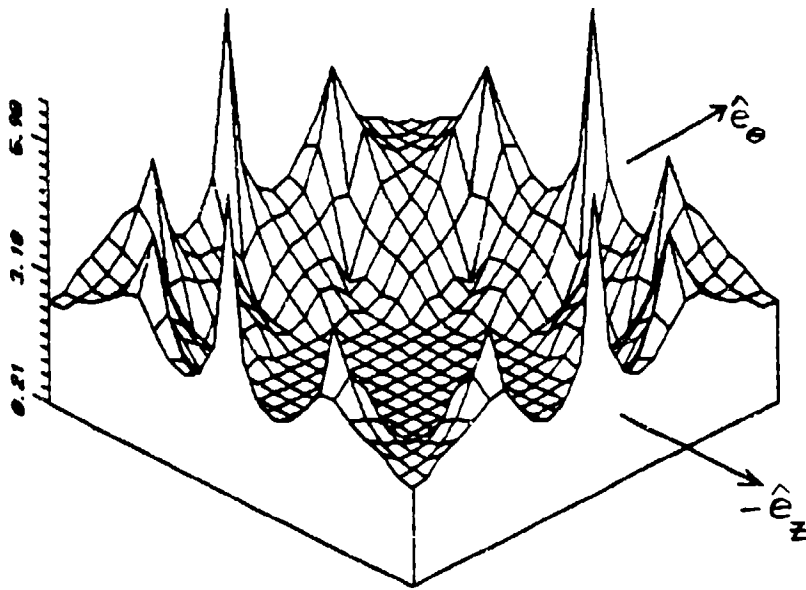
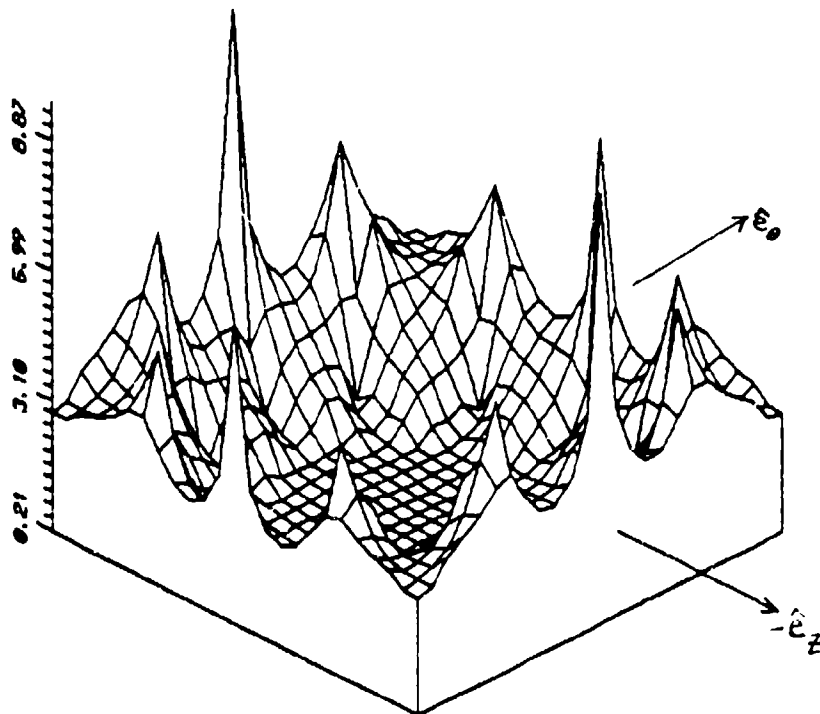


Figure 13. Rectangular Plane Configurations



INITIALLY



MOVED 1/3 ORBIT

Figure 14. Rectangular Plane HPBW Contours

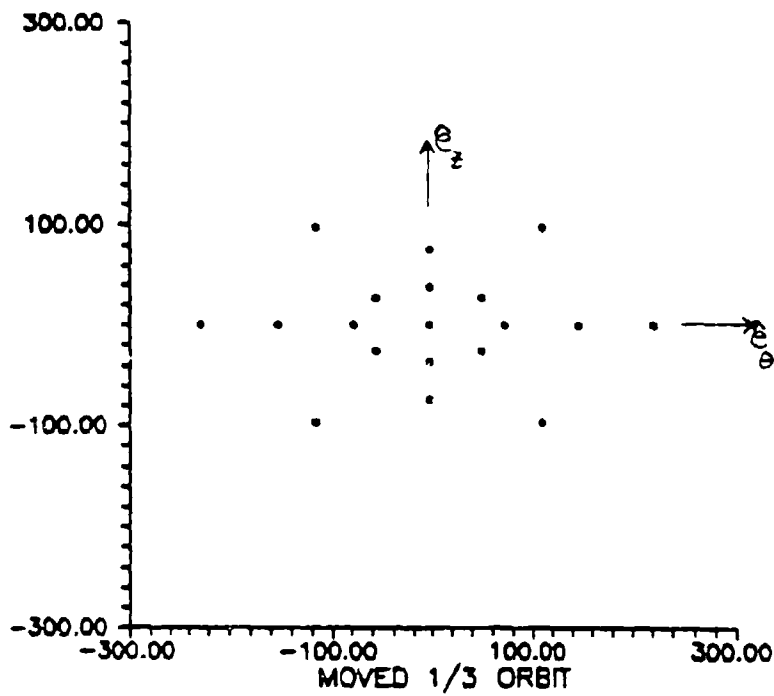
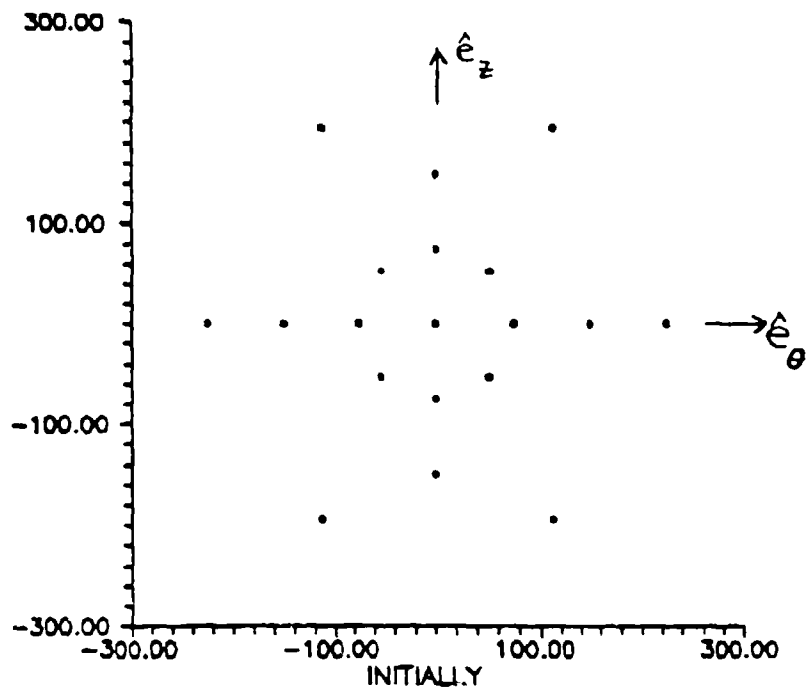
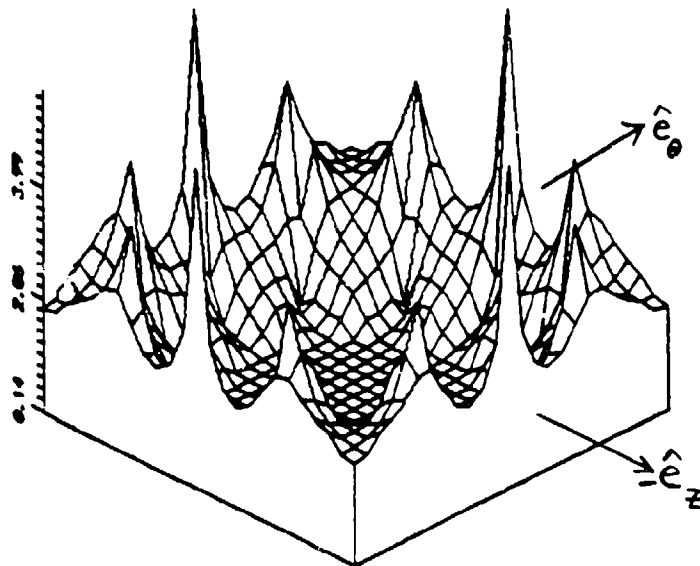
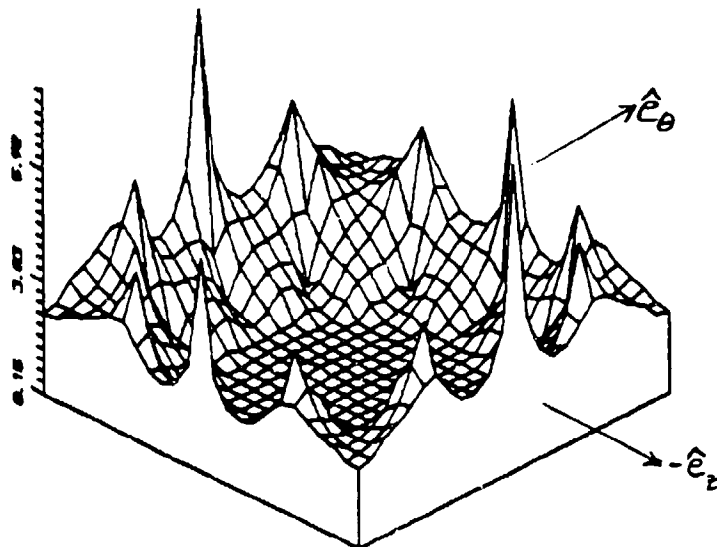


Figure 15. Disk Array Configurations



INITIALLY



MOVED 1/3 ORBIT

Figure 16. Disk Array HPBW Contours

Cone Array The cone array was made by putting the rings of the 19 element disk array at increasing radial levels. Figure 17 shows the relative positions of the cone array. Because of the \hat{e}_x displacements, the elements moved more in the \hat{e}_θ direction than with the disk array. Figure 18 shows the HPBW contours. As with the planar arrays, the HPBW increased when the beam was pointed away from the downward radial direction.

Sphere Instead of a specific configuration, a purely random displacement was tried. A sphere of twenty emitters was used. The random sphere was chosen because it would reflect the most general orbit placement. The satellites could be released from a booster in the general area and given enough ΔV to ensure adequate spacing. The positions of the emitters in the sphere are shown in Figure 19. The HPBW contour plots are shown in Figure 20.

Figure 20 shows the sphere had very similar HPBWs in all directions below the array. Unlike the planar arrays, the sphere would not be limited to certain angles of operation. For a three-dimensional array in space, the capability to have the same beamwidth in all directions would be ideal. The array could be used to track targets almost from horizon to horizon.

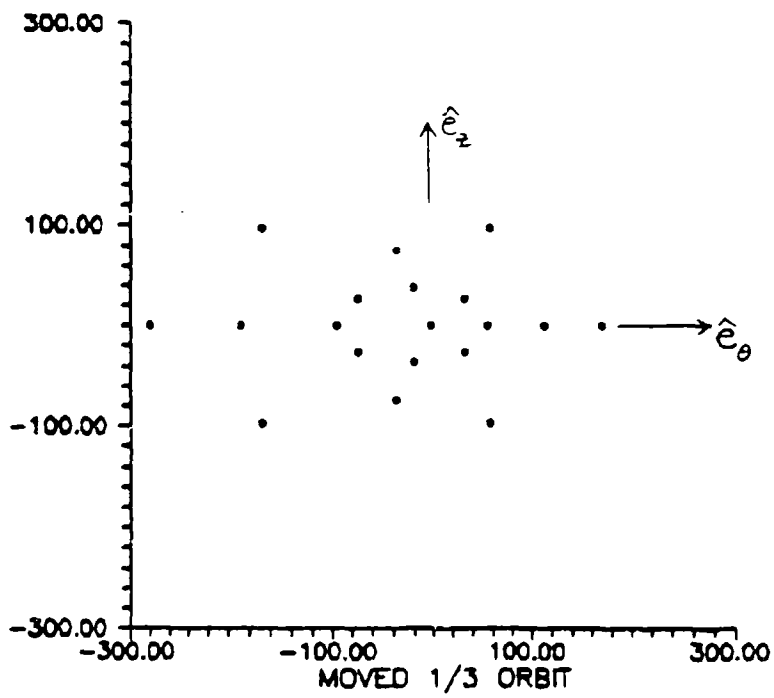
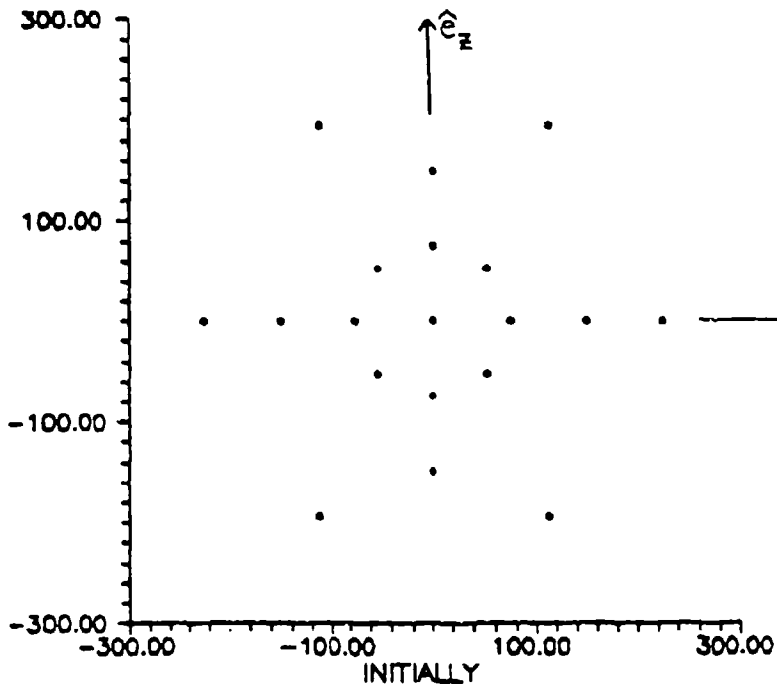
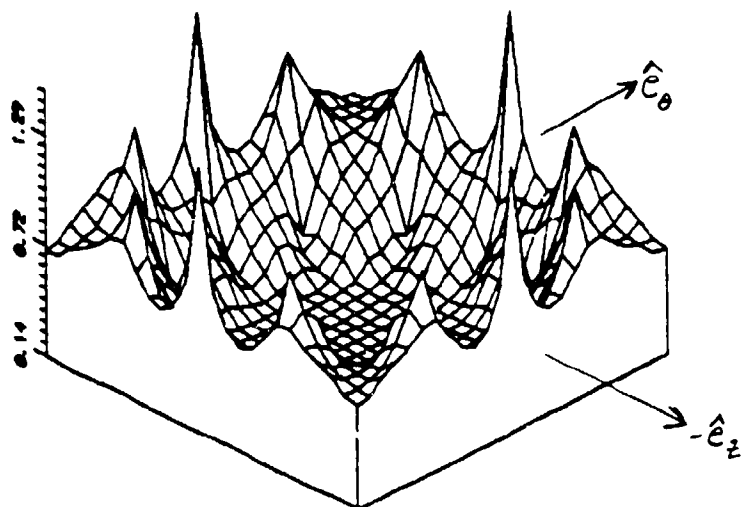
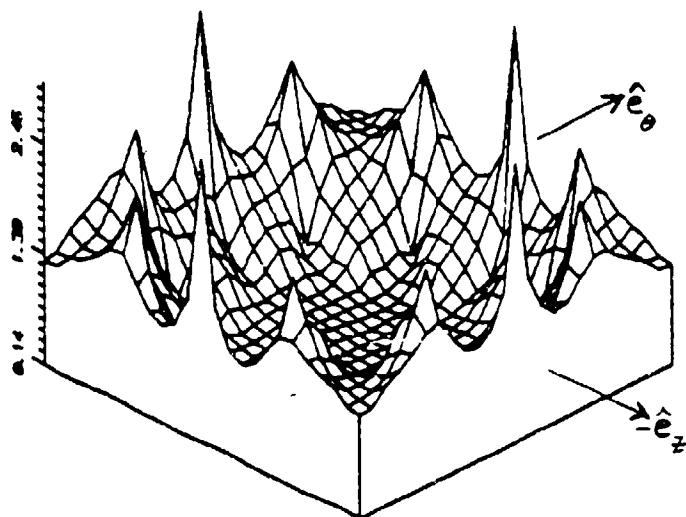


Figure 17. Cone Array Configurations



INITIALLY



MOVED 1/3 ORBIT

Figure 18. Cone Array HPBW Contours

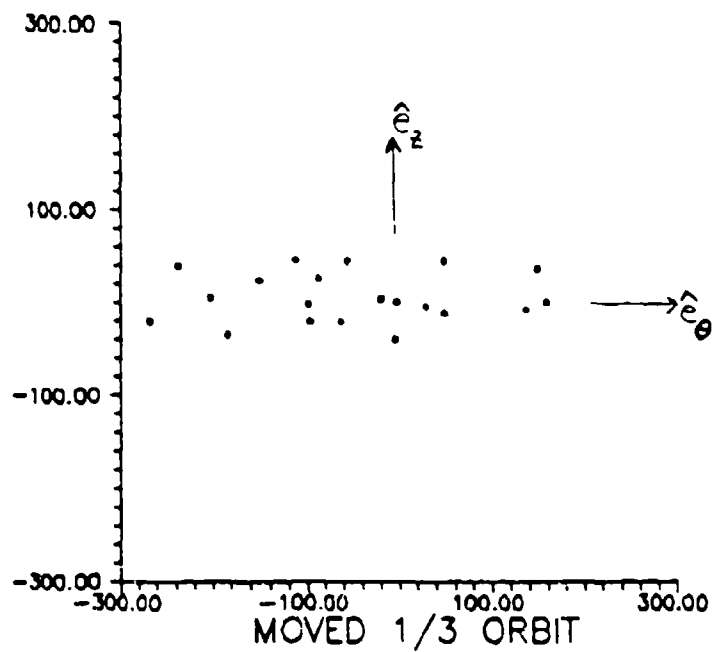
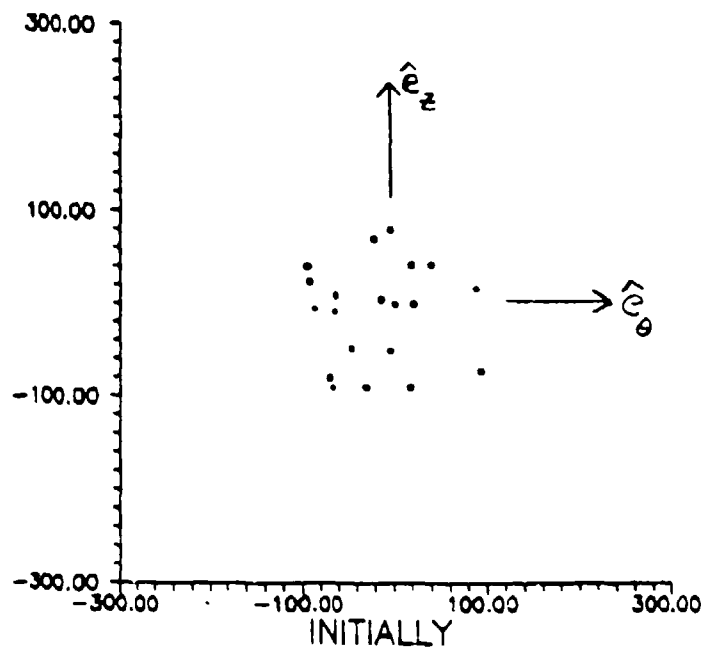
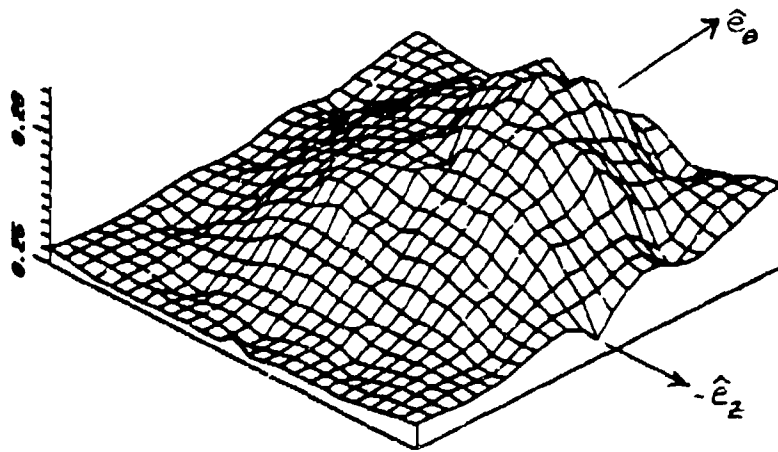
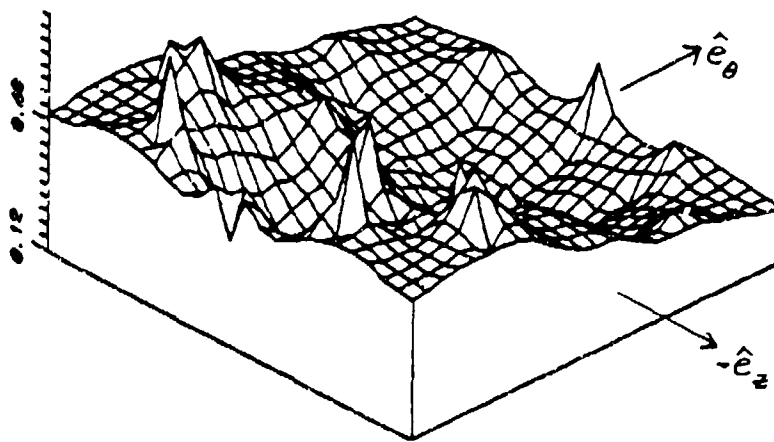


Figure 19. 20 Emitter Sphere Configurations



INITIALLY



MOVED 1/3 ORBIT

Figure 20. 20 Emitter Sphere HPBW Contours

Sphere Analysis

Because the sphere had good beamwidths in almost all directions, it was chosen to use for further analysis. The next step was to modify different spheres to determine the effects of changing the various input parameters. Although there were many input parameters, only a few actually caused the HPBW to change. The input parameters that were varied were the altitude, wavelengths, number of emitters and relative positions of the emitters.

The altitude was found to have no effect on the HPBW. One array was run with varying altitudes and moved 1/3 an orbit each time. The relative positions and HPBW contours were the same in each case. This result was correct because in equation (41), r_0 was not a factor in determining the electric field. Also, equations (27) show that the altitude was not a variable and, therefore, did not effect the relative positions. The altitude was therefore, eliminated as a limiting parameter.

The wavelength had a direct effect on the HPBW. The half-power beamwidth could be approximated by equation (52) because the radar analysis was in the far-field and the configurations were sparsely spaced arrays with the aperture dimension D , much greater than one wavelength. Equation (52) yields the HPBW in radians (7:362-363).

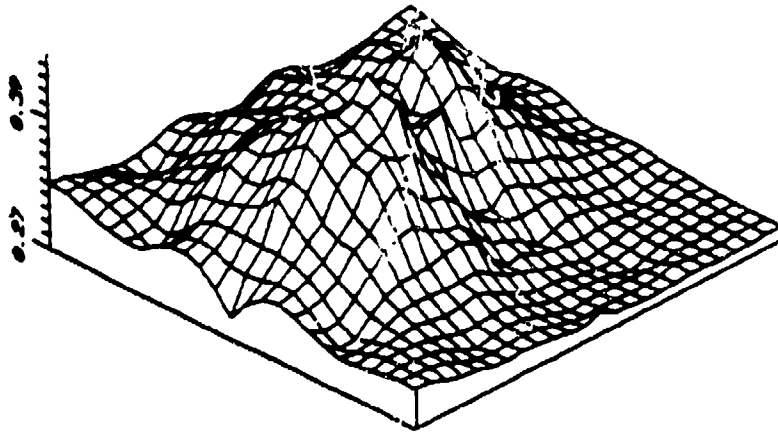
$$\text{HPBW} \approx \lambda / D \quad (52)$$

Equation (52) shows the HPBW was inversely proportional to the size of the array. For a given wavelength, the larger the array, the smaller the HPBW. The relative dimensions were normalized to wavelengths by setting the wavelength equal to one.

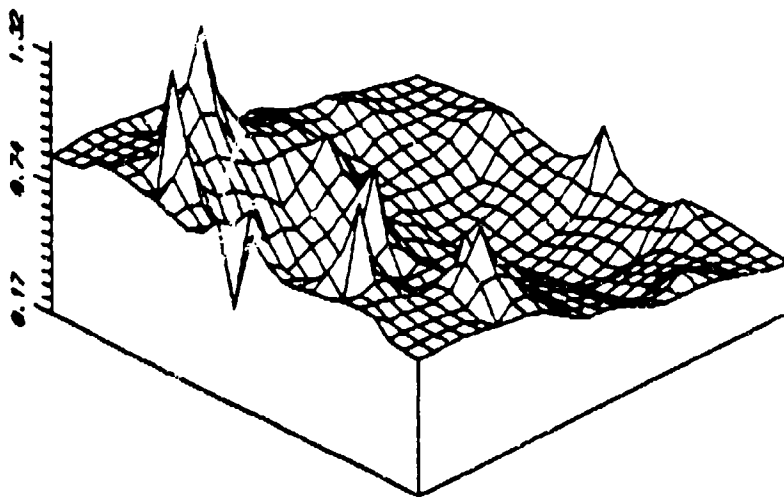
Two spheres with different radial lengths were run to show the effect due to the size of the array. The initial radius of sphere 1 was 75λ and the radius of sphere 2 was 200λ . The initial and 1/3 orbit cases were run and Table II lists the minimum and maximum HPBW values. Figures 21 and 22 show the HPBW contours. As expected, the size of the HPBW decreased with the larger array. To show the similarity, the contour plots for sphere 2 were scaled to twice the values of sphere 1. Although the values of the HPBWs changed, the shapes of the contours did not.

Table II. Minimum and Maximum HPBW Values

Sphere	Half-power Beamwidth (deg)	
	Minimum	Maximum
1 (0)	0.2724	0.4570
1 (1/3)	0.1639	1.6141
2 (0)	0.1022	0.1714
2 (1/3)	0.0615	0.6005

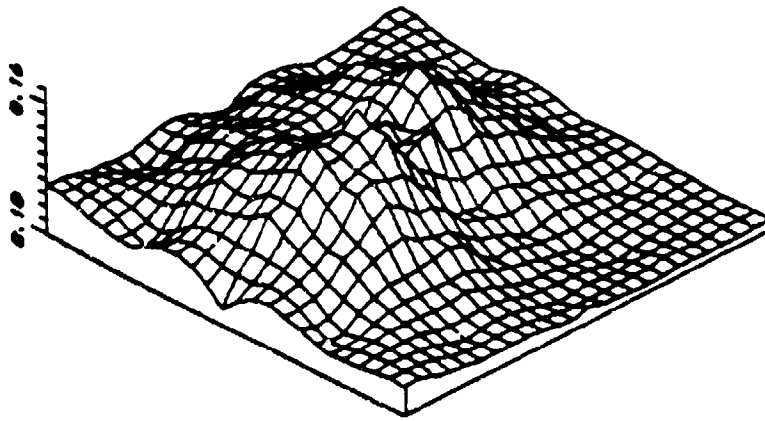


INITIALLY

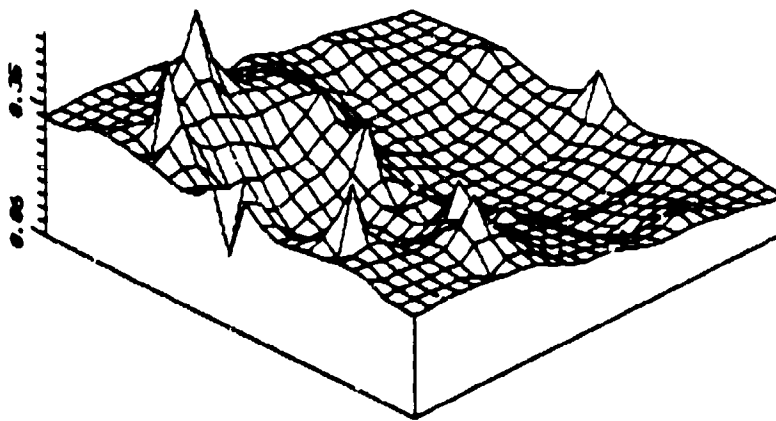


MOVED 1/3 ORBIT

Figure 21. Sphere 1 HPBW Contours



INITIALLY



MOVED 1/3 ORBIT

Figure 22. Sphere 2 HPBW Contours

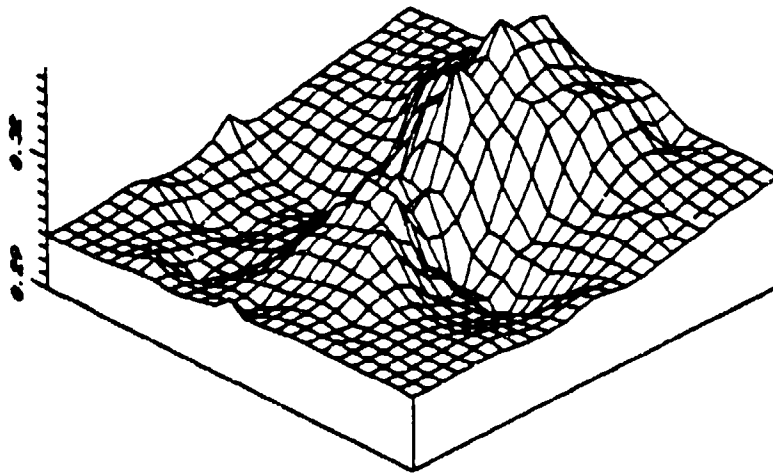
For all the spheres there were spikes in the HPBW contour plots of the 1/3 orbit configurations. A possible cause for these spikes was the specific placement of the emitters. Another cause might have been the number of emitters in the sphere. A third possibility was the spikes were just the result of the orbit motion.

For the first case, three other spheres with the same number of emitters were run but with different random number seeds. The seed number caused the random generating routine to make different initial positions.

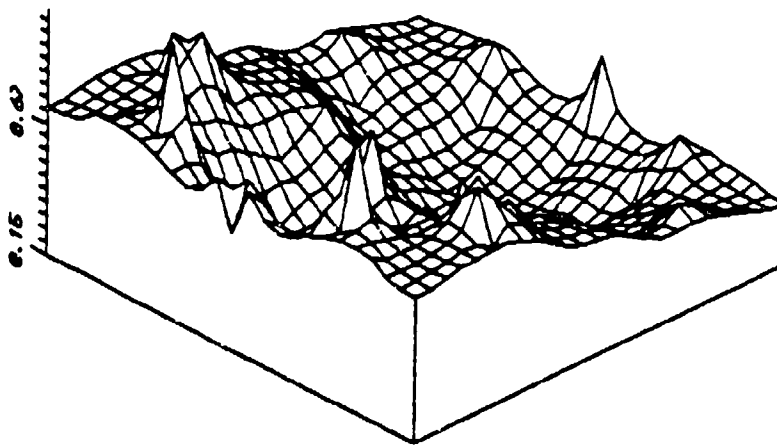
The HPBW contour plots for spheres A, B, and C are in Figures 23, 24, and 25. The scaling on the contour maps was not all the same. Some plots were scaled as much as 20 times to enhance the small changes in the beamwidth. The actual minimum and maximum HPBW are given in Table III.

Table III. Three Random Sphere Beamwidths

Sphere	Half-power Beamwidth (deg)	
	Minimum	Maximum
Before		
A	0.2863	0.3353
B	0.2092	0.4841
C	0.2337	0.4869
After		
A	0.1458	1.3013
B	0.1112	1.5616
C	0.2079	1.0755

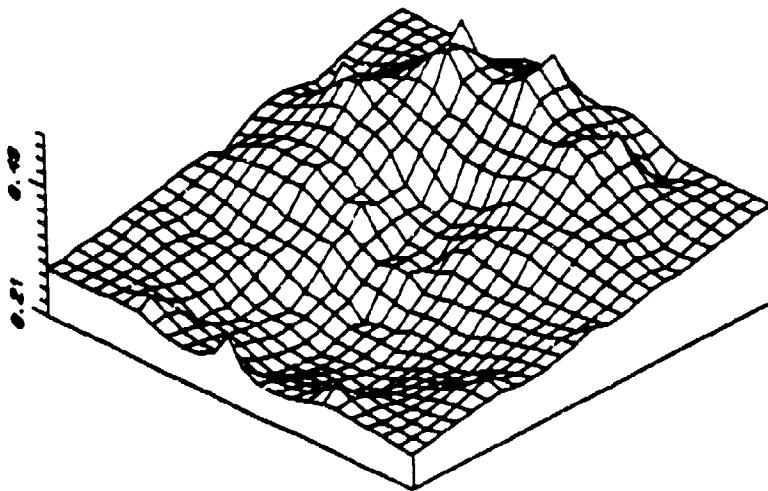


INITIALLY

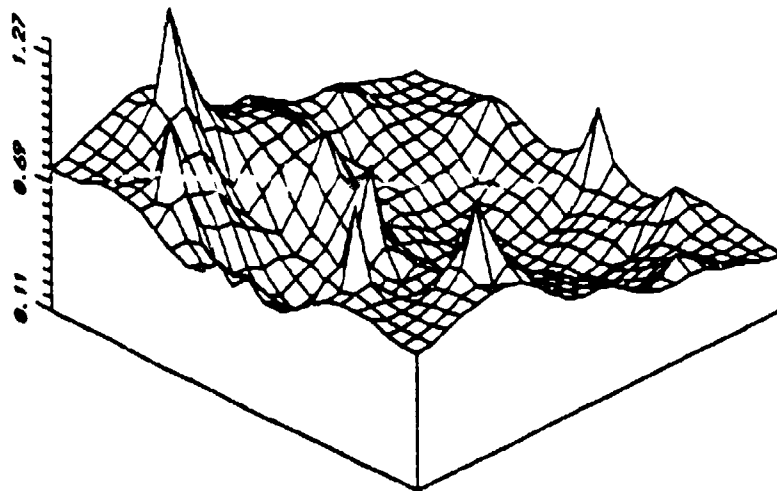


MOVED 1/3 ORBIT

Figure 23. Random Sphere A HPBW Contours

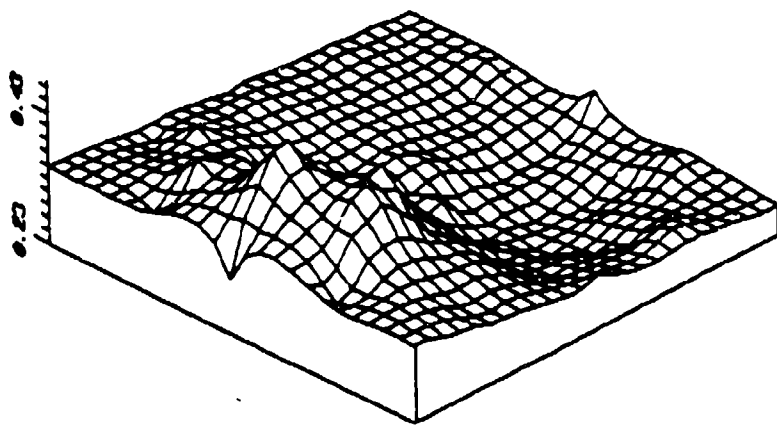


INITIALLY

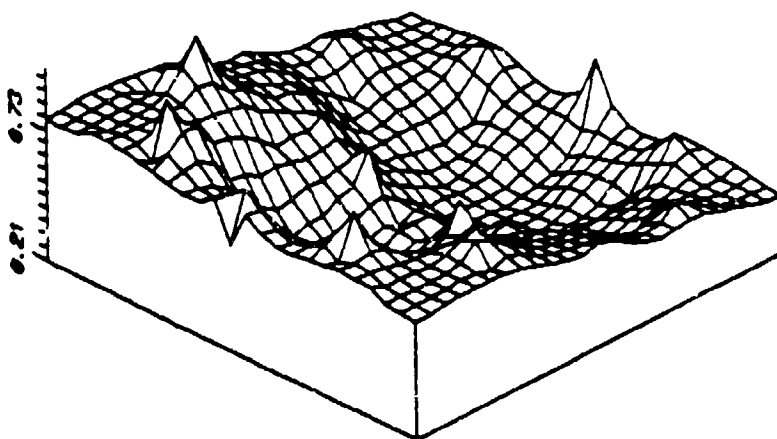


MOVED 1/3 ORBIT

Figure 24. Random Sphere B HPBW Contours



INITIALLY



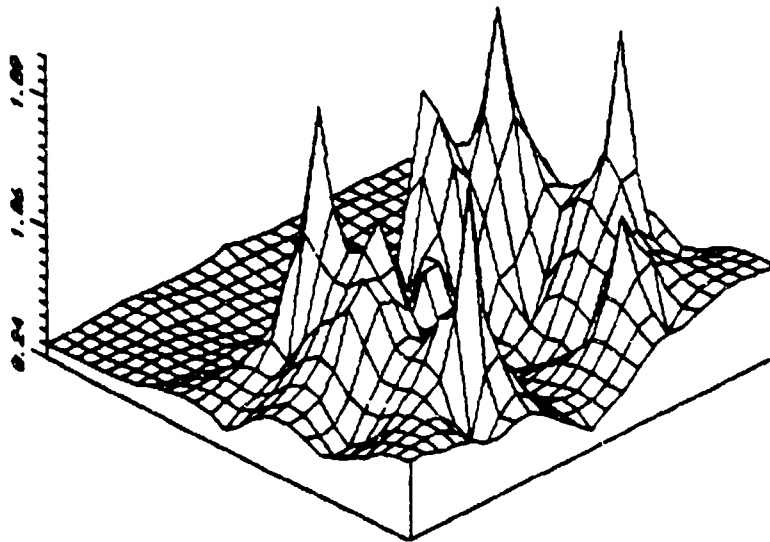
MOVED 1/3 ORBIT

Figure 25. Random Sphere C HPBW Contours

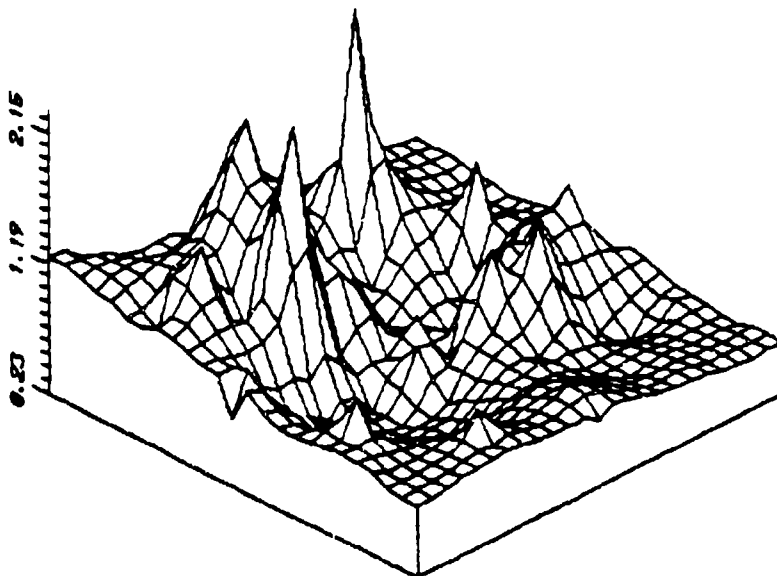
The HPBW figures show each array was initially unique. Spheres A and B had larger HPBW values in the forward \hat{e}_θ direction. After moving 1/3 an orbit, the beamwidth improved in the forward direction and was worse towards the rear edges. All the spikes appeared in the general area to the left rear of the center.

The final modification was to determine the effect of the density of the sphere on the HPBW. Three other spheres with different numbers of emitters were run. The spheres had 5, 25, and 200 emitters. Figures 26, 27, and 28 show the HPBW contours. The figures show the beamwidth depended strongly on the number of emitters in the sphere. In certain directions, the HPBW increased because of the positions of the emitters. In those directions, the projected aperture dimension D decreased.

As Figure 26 shows, the 5 element sphere was poor in many directions. When the number of emitters was increased, the configuration more resembled a solid sphere with the projections in all directions being nearly identical. The HPBWs, therefore, were small and similar in all directions.

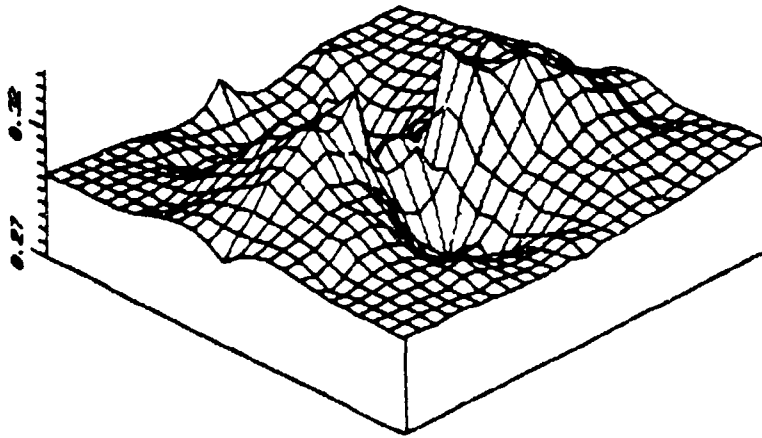


INITIALLY

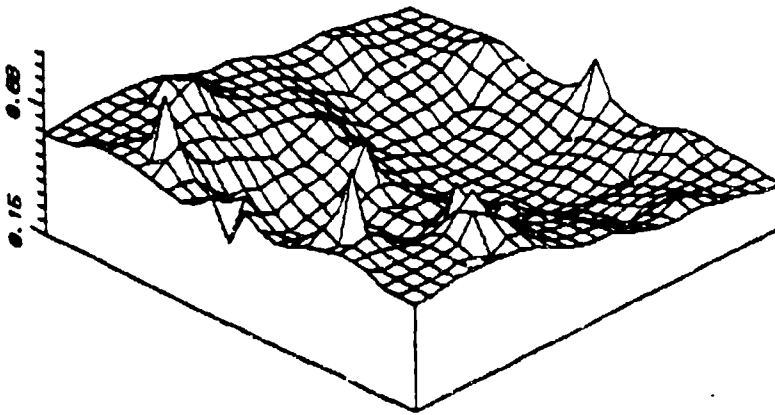


MOVED 1/3 ORBIT

Figure 26. Five Element Sphere HPBW Contours

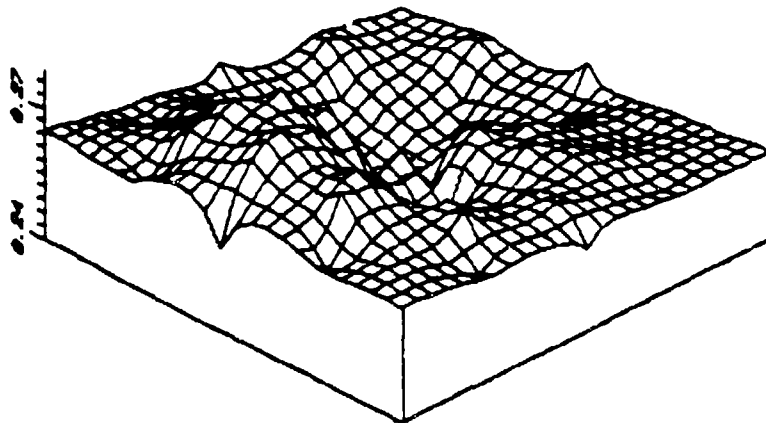


INITIALLY

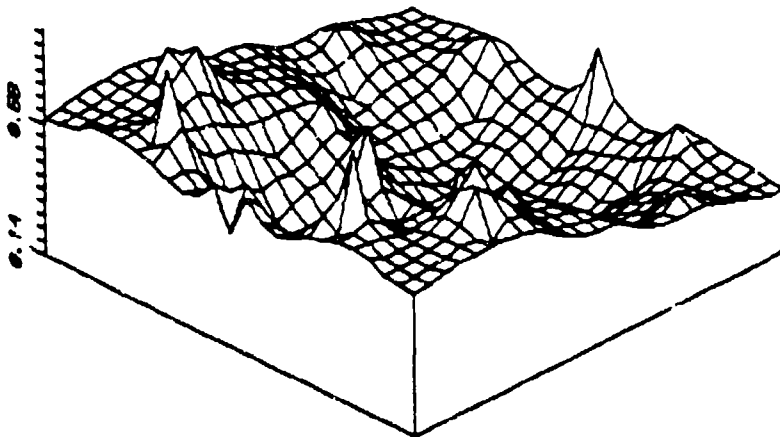


MOVED 1/3 ORBIT

Figure 27. Twenty-five Element Sphere HPBW Contours



INITIALLY

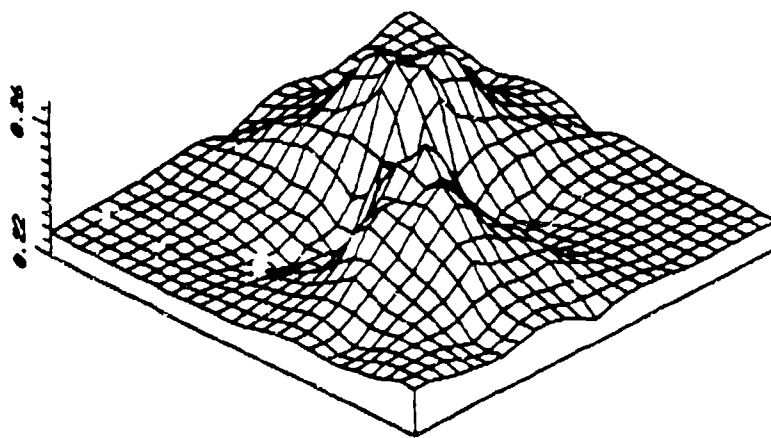


MOVED 1/3 ORBIT

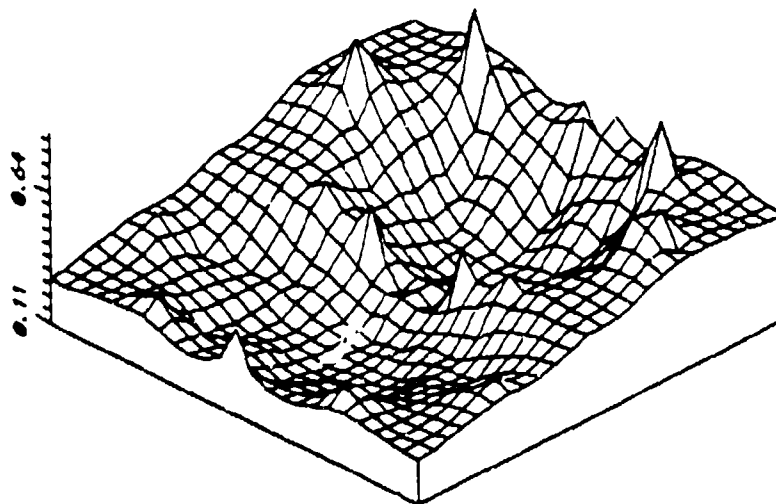
Figure 28. 200 Element Sphere HPBW Contours

For each input modification analyzed, the spikes were present. The spikes, therefore, appeared to have been related to the motion of the array. Another sphere, was used to show the change of the HPBW at several points in the orbit. The sphere, Sphere X, had 20 elements. The HPBW contour plots were generated for each 1/6th of an orbit and are shown in Figures 29 - 32.

The figures show the degraded HPBW began in the forward \hat{e}_θ direction and progressed to the rear \hat{e}_θ direction as the array moved through one half of an orbit. After half of an orbit the HPBW values returned to the original 0.24 - 0.27 degree range. However, the humps moved indicating the directions of poor beamwidths made a 180 degree shift from the front to the rear. The reason for this shift was that after half an orbit, the entire array had reversed itself. As the array returned to its original positions, the HPBW values repeated the patterns in moving from the front to the rear.

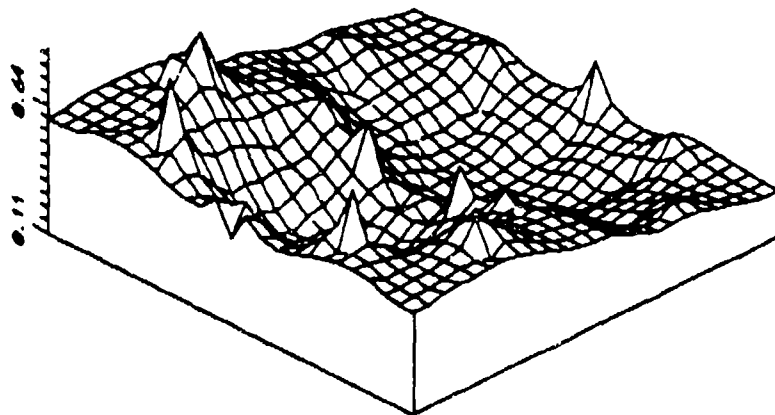


INITIALLY

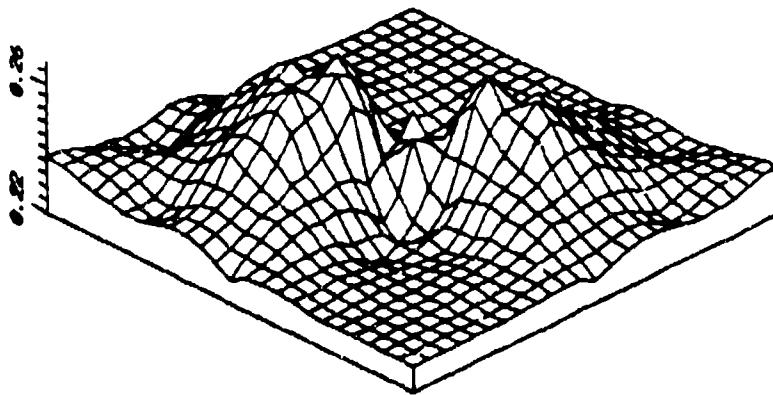


MOVED 1/6 ORBIT

Figure 29. Early Orbit HPBW Contours for Sphere X

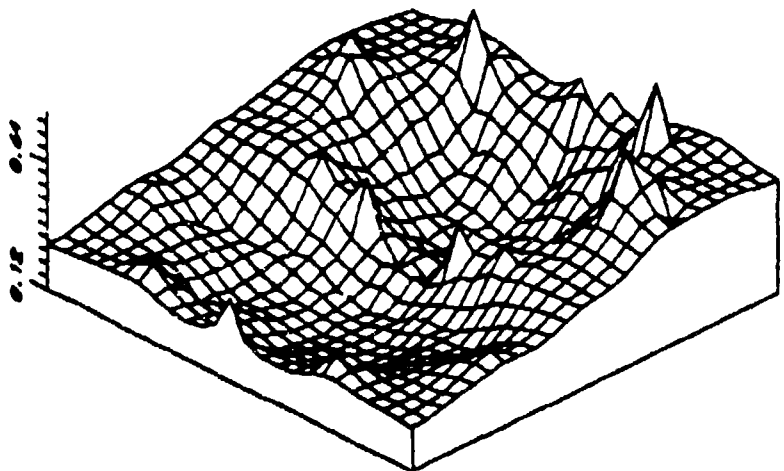


MOVED 1/3 ORBIT

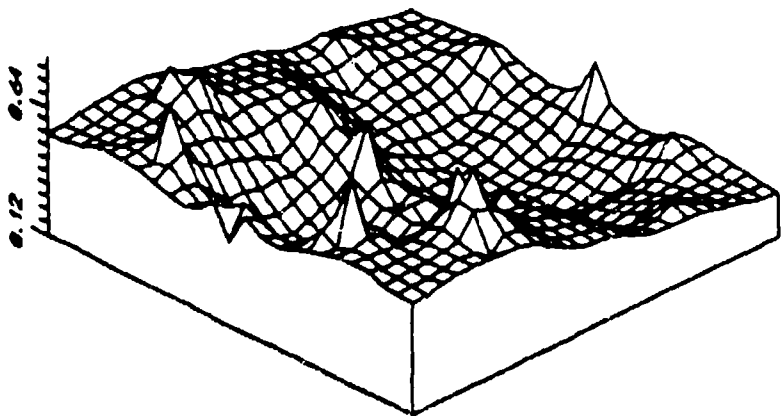


MOVED 1/2 ORBIT

Figure 30. Mid-Orbit HPBW Contours for Sphere X

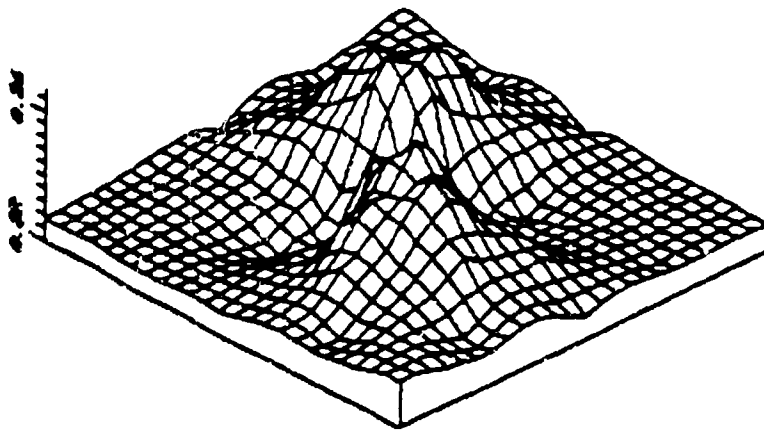


MOVED 2/3 ORBIT



MOVED 5/6 ORBIT

Figure 31. Late Orbit HPBW Contours for Sphere X



ONE ORBIT

Figure 32. Final HPBW Contour for Sphere X

Conclusions and Recommendations

Summary

The most useful configuration was found to be a sphere of randomly spaced emitters. The sphere provided useful half-power beamwidths in all directions below the array. The planar arrays' regions of useful beamwidths were limited to just below the configurations. Because the random sphere could essentially look from horizon to horizon, it would require fewer emitters to cover a large area than a planar array. The random sphere of emitters would be easier to construct than the other arrays because the initial positions would be less stringent.

The value of the HPBW in a given direction depended on the number and relative placement of the emitters. The number of necessary emitters was not large. The expected value of beamwidth, λ/D , was achieved in all directions with about twenty emitters. Five emitters was too few and 200 was overkill.

An array was assumed to be in two-body motion. To keep the emitters from forever drifting apart, there was one limiting assumption. The initial velocity in the \hat{e}_θ direction had to be proportional to the initial radial displacement of the emitter, (equation 46). As an array progressed in its orbit, the oscillatory motion caused the

directions of poor beamwidths to predictably shift. The half-power beamwidths actually improved in certain directions and only slightly degraded in others.

Recommendations

Although only spheres were analyzed for this thesis, other three-dimensional shapes could be evaluated. The regions of antenna coverage could be varied by using ellipsoids with different axis lengths. Certain orientations of the ellipsoid could improve the half-power beamwidths but the effect of the motion must be considered.

For this thesis, the emitters were assumed to be point source radiators. Follow on work could use other types of space qualified radar emitters to predict the effects of orbital motion on the capabilities of the arrays.

Appendix: Computer Program

```
program newpat
integer ttt,w
real nu,mu,min,lam,Eo
character*12 Outfile, infile
common ro,n,lam,nn,nu,radius,alt,Eo
dimension R(240,3),V(240,3),ro(240,3),vo(240,3)
write(*,5)
5 format(1x,'ENTER THE NAME OF THE LOCATION OUTPUT FILE')
read (*,10) Outfile
10 format(a12)
open (unit=2,file=Outfile,status='new')
write(*,12)
12 format(1x,'ENTER THE NAME OF THE FILE FOR INPUT')
read (*,10) infile
open (unit=5,file=infile,status='old')
c
c THE NUMBER OF ARRAY ELEMENTS IS N
read(5,15) n
write(2,15) n
15 format(i4)
c INPUT THE WAVELENGTH (lam) IN KILOMETERS
c
read (5,20) lam
20 format(f15.7)
c
c INPUT THE ALTITUDE OF THE CENTER IN KILOMETERS
read(5,20) alt
c
c INPUT MAXIMUM DISPLACEMENTS IN Er AND Ez DIRECTIONS
c THESE MUST BE IN KILOMETERS
read(5,20)drmax
read(5,20)dzmax
c
radius = 6378.145 + alt
mu = 3.986012e05
vcir = sqrt(mu/radius)
nn = sqrt(mu/(radius**3))
period = 2.*3.1415926535/nn
c
c SPECIFY THE TYPE OF ARRAY TO USE'
c PICK ONE OF THE FOLLOWING CASES'
c 1) RECTANGULAR PLANE'
c 2) HEXOGONAL PLANE'
c 3) CIRCULAR PLANE'
c 4) ELLIPTICAL PLANE'
c 5) RANDOMLY SPACED ELLIPSOID'
read (5,25) ick
25 format(i4)
c
```

```

c      DETERMINE THE SPACING OF THE ELEMENTS WR2 THE CENTER
c
      if (ick.eq.1) then
          call rectangle
      else if (ick.eq.2) then
          call hexogon
      else if (ick.eq.3) then
          call circ
      else if (ick.eq.4) then
          call platter
      else if (ick.eq.5) then
          call blob
      end if

c
      min = 0.0
      write(2,35) min
35     format(e15.7)
      do 50 i=1,n
          write(2,40)i,ro(i,1),ro(i,2),ro(i,3)
40     format(1x,i4,3(2x,e15.7))
50     continue

c
      write(*,55)
55     format(1x,'INITIALIZING R() FROM RO()')
      do 65 i=1,n
          do 60 j=1,3
              r(i,j) = ro(i,j)
60         continue
65     continue

c
      write(*,70)
70     format(1x,'INITIALIZING VO()')
      do 75 i = 1,n
          vo(i,2) = -2.0*nn*ro(i,1)
75     continue
      do 80 i = 1,n
          vo(i,3) = nn*dzmax
          vo(i,1) = nn*(drmax - 4.0*ro(i,1))-(2.0*vo(i,2))
80     continue
c      write(2,85) alt
85     format(1x,'ALTITUDE = ',e15.7)
c      write(2,90) drmax
90     format(1x,'DRMAX = ',e15.7)
c      write(2,95) dzmax
95     format(1x,'DZMAX = ',e15.7)
c      do 97 i=1,n
c      write(2,96) i,vo(i,1),vo(i,2),vo(i,3)
c96     format(1x,i4,3(2x,e15.7))
c97     continue
      delmin = period/3.0/60.0
      do 125 boo =1,2
          call efield(r,min)
          min = min + delmin
          call moveit(r,v,min,vo)

```

```

write(2,100) min
100   format(e15.7)
c     write(2,105)
c105   format(1x,'NEW POSITIONS'/)
       do 110 i = 1,n
       write(2,107)i,r(i,1),r(i,2),r(i,3)
107   format(1x,i4,3(2x,e15.7))
110   continue
125   continue
       post = 9999.0
       write(2,144) post
       write(*,145)
144   format(e15.7)
145   format(1x,'FINISHED')
close(unit=5)
close(unit=2)
stop
end

c
subroutine rectangle
common ro,n,lam,nn,mu,radius,alt,Eo
dimension a(240),b(240),ro(240,3)
real lam
       do 220 i=1,n
       read(5,200) a(i),b(i)
200   format(2f10.5)
220   continue
c
c   INPUT THE TILT ANGLE FOR THE PLANE (DEGREES)'
c   TOP GOING AWAY IS POSITIVE'
c
       read (5,230) alpha
230   format(f10.5)
       alpha = alpha*3.14159/180.0
       ss = sin(alpha)
       cc = cos(alpha)
c
c   DISTANCES ARE MULTIPLES OF THE SIGNAL WAVELENGTH
c
c   ENTER SCALE FACTOR (d) FOR SPACING (2*LAM, ETC)'
       read (5,230) scale
c
       do 240 i=1,n
       ro(i,1) = b(i)*ss*scale*lam
       ro(i,2) = -a(i)*scale*lam
       ro(i,3) = b(i)*cc*scale*lam
240   continue
       return
       end
c
subroutine hexogon
return
end
subroutine circ

```

```

return
end

c
subroutine platter
common ro,n,lam,nn,mu,radius,alt,Eo
dimension ro(240,3)
integer nrings
psi = 0.0
j = 0
c
A AND DEPTH MUST BE IN KILOMETERS
read(5,250) a,ecc,nrings
250 format(2(f10.3),i5)
do 260 i =1,nrings
read(5,252) ringfac,inr,depth
252 format(f10.3,i5,f10.3)
dpsi =360.0/inr
ao = a * ringfac
bo = ao * sqrt(1.-ecc**2)
do 265 d=1,inr
j = j+1
ppsi = psi * 3.14159/180.0
ro(j,2) = -ao*cos(ppsi)
ro(j,3) = bo*sin(ppsi)
ro(j,1) = depth
psi = psi + dpsi
265 continue
260 continue
return
end

c
subroutine blob
common ro,n,lam,nn,mu,radius,alt,Eo
dimension ro(240,3)
real legr,legthe,legz,numb1,numb2,numb3,jj,kk,jo,ko
integer y,w
c
THIS ROUTINE GENERATES RANDOM LOCATIONS
c
FOR THE ARRAY ELEMENTS
c
c
INPUT MAXIMUM LENGTHS OF EACH AXIS OF THE ELLIPSOID
c
c
THE AXIS LENGTHS ARE IN KILOMETERS"
c
c
Y IS ANY ODD NUMBER BETWEEN 0 AND 67108863
c
read (5,300) y
300 format(i8)
read (5,311) legr
read (5,311) legthe
read (5,311) legz
311 format(f15.7)
c
establishing the center
ro(1,1) = 0.0
ro(1,2) = 0.0
ro(1,3) = 0.0

```

```

do 320 i = 2,n
  numb1 = rand(y)
  ro(i,1) = legr * (2*numb1-1)
  numb2 = rand(y)
  ro(i,2) = legthe * (2*numb2-1)
  numb3 = rand(y)
  ro(i,3) = legz * (2*numb3-1)
320  continue
return
end

c
function rand(iy)
c
c pseudo random number generator on interval (0,1)
c Collected Algorithms of the CCM #266
c assumes 2**31 integer math
c iy is odd integer between 0 and 67108863
c don't change it after first call
c
dimension k(3)
data k/25,25,5/
c
do 400 i = 1,3
  iy = k(i)*iy
  iy = iy - (iy/67108864)*67108864
400  continue
  rand = real(iy)/67108864.0
return
end

c
subroutine efield(r,min)
common ro,n,lam,nn,mu,radius,alt,Eo
real lpr,lpz,lor,loz,lot,lpt,jj,kk,jo,ko,lam,min
real aa,bb,zz,diffp,diffa,ea,ep,cek,mu,nn
character*12 outname,outfile
dimension doto(240),dotp(240),direct(40,80)
dimension ro(240,3),r(240,3)
c
write(*,500)
c500  format(1x,'Enter the name of the Efield output file')
c
read(*,510) outname
c510  format(a12)
c
open (unit=7,file='field.out',status='new')
open (unit=8,file='plotfile',status='new')
c
write(7,515) min
c
write(8,515) min
515  format(1x,e15.7)
c
c
c EACH ELEMENT IS ASSUMED TO BE AN ISOTROPIC POINT
c SOURCE EMITTING ITS ENERGY IN PHASE
c
c ALL ELEMENTS EMIT THE SAME IN-PHASE AMPLITUDE, Eo
c
Eo = 1.0
icount = 0

```

```

    itag = 1
    do 600 j=0,90,15
      jj = j
      jo = jj
c   this needs to go 0 to 360
      do 590 k=0,360,30
        sum1 = 0.0
        sum2 = 0.0
        kk = k
        ko = kk
        if(k.eq.360) then
          goto 590
        end if
        phi = jj * 3.1415926535/180.0
        the = kk * 3.1415926535/180.0
        lor = -sin(phi)
        lot = cos(phi)*cos(the)
        loz = cos(phi)*sin(the)
        lpr = lor
        lpt = lot
        lpz = loz
        do 520 i=1,n
          doto(i) = (r(i,1)*lor + r(i,2)*lot +
                    r(i,3)*loz)*6.2831853/lam

          dotp(i) = (r(i,1)*lpr + r(i,2)*lpt +
                    r(i,3)*lpz)*6.2831853/lam

          sum1 = sum1 + cos(dotp(i)-doto(i))
          sum2 = sum2 + sin(dotp(i)-doto(i))
520      continue
          emax = Eo*sqrt(sum1*sum1 + sum2*sum2)
          sum1 = 0.0
          sum2 = 0.0
c   ***** STEP DOWN SEARCH *****
          delta = 1.0
          jcount = 0
999      if(jcount.ge.360) then
            band = 1.0 - ratio
            if(band.lt.0.000000001) then
              hpbw1 = 360.0
            else
              hpbw1 = 5555.5555
            end if
            jj = jo
            jcount = 0
          goto 1001
        end if
        sum2 = 0.0
        sum1 = 0.0
        phi = jj * 3.1415926535/180.0
        the = kk * 3.1415926535/180.0
        lpr = -sin(phi)
        lpt = cos(phi)*cos(the)

```

```

lpz = cos(phi)*sin(the)
do 530 i = 1,n
dotp(i) = (r(i,1)*lpr + r(i,2)*lpt +
           r(i,3)*lpz)*6.2831853/lam

    sum1 = sum1 + cos(dotp(i)-doto(i))
    sum2 = sum2 + sin(dotp(i)-doto(i))
530 continue
ENOW = Eo*sqrt(sum1*sum1 + sum2*sum2)
sum1=0.0
sum2=0.0
ratio = ENOW/emax
differ = ratio - 0.7071
if(differ.gt.0.0) then
    jj = jj + delta
    jcount = jcount + 1
    goto 999
end if
c END STEP DOWN SEARCH
c
c*****
c BISECTION SEARCH FOR HPBW1 BETWEEN JJ-1.0 AND JJ
c DOING THIS FOR JJ ONLY NOW
1155 aa = jj - delta
    bb = jj
    tol = 0.00001
    nomax = 50
    icount = 1
3333 if(icount.lt.nomax) then
    flag = 1
    zz = aa
    goto 222
5555 EA = ENEW
7777 p = aa + (bb - aa)/2.0
    zz = p
    flag = 2
    goto 222
4444 EP = ENEW
    diffp = ((EP/emax) - 0.70710678)
    chek = abs(bb-aa)
    if(abs(diffp).lt.tol.or.chek.lt.tol) then
        hpbw1 = 2.0*abs(jo-p)
        jj = jo
        icount = 0
        goto 1001
    end if
    diffa = ((EA/emax) - 0.70710678)
    if(diffa*diffp.gt.0.0) then
        aa = p
    else
        bb = p
    end if
    icount = icount + 1
    goto 3333

```

```

        else
            goto 8888
        end if
c *****
222  sum1 = 0.0
    sum2 = 0.0
    phi = zz * 3.1415926535/180.0
    the = kk * 3.1415926535/180.0
    lpr = -sin(phi)
    lpt = cos(phi)*cos(the)
    lpz = cos(phi)*sin(the)
    do 550 i = 1,n
        dotp(i) = (r(i,1)*lpr + r(i,2)*lpt +
                    r(i,3)*lpz)*6.2831853/lam
        sum1 = sum1 + cos(dotp(i)-doto(i))
        sum2 = sum2 + sin(dotp(i)-doto(i))
550  continue
    ENEW = Eo*sqrt(sum1**2 + sum2**2)
c *****
    if(flag.eq.1) then
        goto 5555
    end if
    if(flag.eq.2) then
        goto 4444
    end if
c  DIDN'T WORK
8888 hpbw1 = 2222.2222
c *****
1001 continue
c  write(7,560) jo,ko,hpbw1
560  format(1x,2(2x,f6.1),2x,e15.7)
c  sending data to the file to make the plot
    tto = ko*3.1415926535/180.0
    ppo = jo*3.1415926535/180.0
    xxx = cos(ppo)*cos(tto)
    yyy = cos(ppo)*sin(tto)
    zzz = hpbw1
    write(8,570) xxx,yyy,zzz
570  format(1x,3(2x,e15.7))
    jj=jo
590  continue
c  write(*,595)
c595  format(1x,'WORKING')
600  continue
    write(*,610)
610  format(1x,'FINISHED DOING THE E-FIELD')
c  close (unit=7)
c  close (unit=8)
    return
    end

c
c
    subroutine moveit(r,v,min,vo)
    common ro,n,lam,nn,mu,radius,alt,Eo

```

```

dimension phirr(3,3),phirv(3,3),phivr(3,3),phivv(3,3)
dimension ro(240,3),r(240,3),vo(240,3),v(240,3)
real lam,nn,mu,min

c
c      write(*,700)
c700  format(1x,'INPUT THE TIME IN MINUTES TO MOVE')
c      read(*,710) min
c710  format(f15.7)
      t = 60.0*min
      psi = nn*t
c  *****
c      write(*,50) nn,psi
c50   format(1x,'nn = ',e15.7,' psi = ',e15.7)
c  *****
c      do 800 i=1,n
c      write(*,900)i,ro(i,1),ro(i,2),ro(i,3)
c900  format(1x,i4,3(e15.7))
c800  continue
c      do 850 i=1,n
c      write(*,900)i,vo(i,1),vo(i,2),vo(i,3)
c850  continue
c  *****
c      EVALUATING THE FOUR PHI MATRICIES.
      phirr(1,1) = 4.-3.0*cos(psi)
      phirr(1,2) = 0.0
      phirr(1,3) = 0.0
      phirr(2,1) = (6.0*(sin(psi)-psi))
      phirr(2,2) = 1.0
      phirr(2,3) = 0.0
      phirr(3,1) = 0.0
      phirr(3,2) = 0.0
      phirr(3,3) = cos(psi)

c
      phirv(1,1) = sin(psi)/nn
      phirv(1,2) = (2.0*(1.0-cos(psi))/nn)
      phirv(1,3) = 0.0
      phirv(2,1) = (2.0*(cos(psi)-1.0)/nn)
      phirv(2,2) = 4.0/nn*sin(psi)-(3.0/nn*psi)
      phirv(2,3) = 0.0
      phirv(3,1) = 0.0
      phirv(3,2) = 0.0
      phirv(3,3) = sin(psi)/nn

c
      phivr(1,1) = 3.0*nn*sin(psi)
      phivr(1,2) = 0.0
      phivr(1,3) = 0.0
      phivr(2,1) = (6.0*nn*(cos(psi)-1.))
      phivr(2,2) = 0.0
      phivr(2,3) = 0.0
      phivr(3,1) = 0.0
      phivr(3,2) = 0.0
      phivr(3,3) = -nn*sin(psi)

c
      phivv(1,1) = cos(psi)

```

```

phivv(1,2) = 2.*sin(psi)
phivv(1,3) = 0.0
phivv(2,1) = (-2.*sin(psi))
phivv(2,2) = -3.+4.0*cos(psi)
phivv(2,3) = 0.0
phivv(3,1) = 0.0
phivv(3,2) = 0.0
phivv(3,3) = cos(psi)

```

c
c
c

MOVING R(i) and V(i) FORWARD IN TIME

c

```

do 100 i=1,n
sum1=0.0
sum2=0.0
sum3=0.0
sum4=0.0
sum5=0.0
sum6=0.0
do 150 j=1,3
sum1 = sum1 + phirr(1,j)*ro(i,j) + phirv(1,j)*vo(i,j)
sum2 = sum2 + phirr(2,j)*ro(i,j) + phirv(2,j)*vo(i,j)
sum3 = sum3 + phirr(3,j)*ro(i,j) + phirv(3,j)*vo(i,j)
sum4 = sum4 + phivr(1,j)*ro(i,j) + phivv(1,j)*vo(i,j)
sum5 = sum5 + phivr(2,j)*ro(i,j) + phivv(2,j)*vo(i,j)
sum6 = sum6 + phivr(3,j)*ro(i,j) + phivv(3,j)*vo(i,j)
150 continue
r(i,1) = sum1
r(i,2) = sum2
r(i,3) = sum3
v(i,1) = sum4
v(i,2) = sum5
v(i,3) = sum6
100 continue
return
end

```

Bibliography

1. Brookner, Eli "Phased-Array Radars," Scientific American, 252: 94-102 (February 1985).
2. Canan, James W "USAF in the Twenty-first Century," Air Force Magazine, 69: 46-52 (August 1986).
3. Coghlan, Jim "Countering the Cruise Missile," Defense Electronics, 19: 77-86 (September 1987).
4. Greenwood, Donald T. Principles of Dynamics. Englewood Cliffs, New Jersey: Prentice-Hall Inc., 1987.
5. Jordan, Edward C. Electromagnetic Waves and Radiating Systems. Englewood Cliffs, New Jersey: Prentice-Hall Inc., 1960.
6. Kraus, John D. and Carver, Keith R. Electromagnetics (Second Edition). New York: McGraw-Hill Book Company, 1973.
7. Pratt, Timothy and Bostian, Charles W. Satellite Communications. New York: John Wiley and Sons, 1986.
8. Silver, Samuel Microwave Antenna Theory and Design. MIT Radiation Laboratory Series, Volume 12, New York: McGraw-Hill Book Company, 1949.
9. Stutzman, Warren L. and Thiele, Gary A. Antenna Theory and Design. New York: John Wiley and Sons, 1981.
10. Wiesel, William E Jr. Class handout distributed in Mech 532, Fundamentals of Astrodynamics. School of Engineering, Air Force Institute of Technology (AU), Wright-Patterson AFB OH, October, 1987.

VITA

Captain Michael G. Spencer was born on 28 November 1959 in East Lansing, Michigan. He graduated from Herber Hoover High school in Clendenin, West Virginia, in 1978. He attended West Virginia University from which he received the degree of Bachelor of Science in Aerospace Engineering in May 1983. In August 1983, he received his commission in the USAF through the OTS program at Lackland AFB, San Antonio, Texas. His first assignment was at the Head Quarters Foreign Technology Division, Wright-Patterson AFB, Ohio. He served as a foreign space systems analyst until entering the School of Engineering, Air Force Institute of Technology, in June 1987.

Permanent address: 41 Morningside Dr.

Elkview, West Virginia 25071

UNCLASSIFIED

SECURITY CLASSIFICATION OF THIS PAGE

REPORT DOCUMENTATION PAGE

Form Approved OMB No. 0704-0188

1a. REPORT SECURITY CLASSIFICATION UNCLASSIFIED		1b. RESTRICTIVE MARKINGS	
2a. SECURITY CLASSIFICATION AUTHORITY		3. DISTRIBUTION / AVAILABILITY OF REPORT Approved for public release; distribution unlimited	
2b. DECLASSIFICATION / DOWNGRADING SCHEDULE		5. MONITORING ORGANIZATION REPORT NUMBER(S)	
4. PERFORMING ORGANIZATION REPORT NUMBER(S) AFIT/6A/AA/88D-11		7a. NAME OF MONITORING ORGANIZATION	
6a. NAME OF PERFORMING ORGANIZATION School of Engineering	6b. OFFICE SYMBOL (if applicable) AFIT/ENY	7b. ADDRESS (City, State, and ZIP Code)	
6c. ADDRESS (City, State, and ZIP Code) Air Force Institute of Technology (AU) Wright-Patterson AFB, Ohio 45433-6583		9. PROCUREMENT INSTRUMENT IDENTIFICATION NUMBER	
8a. NAME OF FUNDING / SPONSORING ORGANIZATION	8b. OFFICE SYMBOL (if applicable)	10. SOURCE OF FUNDING NUMBERS	
3c. ADDRESS (City, State, and ZIP Code)		PROGRAM ELEMENT NO.	PROJECT NO.
		TASK NO.	WORK UNIT ACCESSION NO.

11. TITLE (Include Security Classification)
EFFECT OF TWO-BODY MOTION ON RADAR BEAM QUALITY FOR VARIOUS DISTRIBUTED SPARSE ARRAY CONFIGURATIONS

12. PERSONAL AUTHOR(S)
Michael G. Spencer, B.S., Capt, USAF

13a. TYPE OF REPORT MS Thesis	13b. TIME COVERED FROM _____ TO _____	14. DATE OF REPORT (Year, Month, Day) 1988 December	15. PAGE COUNT 85
----------------------------------	--	--	----------------------

16. SUPPLEMENTARY NOTATION

17. COSATI CODES			18. SUBJECT TERMS (Continue on reverse if necessary and identify by block number) Distributed Sparse Array
FIELD	GROUP	SUB-GROUP	
22	03		
17	09		

19. ABSTRACT (Continue on reverse if necessary and identify by block number)

Thesis Advisor: Dr. William E. Wiesel
Professor
Department of Aeronautics and Astronautics

J.P. Remienicki
12 Jan 1989

20. DISTRIBUTION / AVAILABILITY OF ABSTRACT <input checked="" type="checkbox"/> UNCLASSIFIED/UNLIMITED <input type="checkbox"/> SAME AS RPT. <input type="checkbox"/> DTIC USERS		21. ABSTRACT SECURITY CLASSIFICATION UNCLASSIFIED	
22a. NAME OF RESPONSIBLE INDIVIDUAL William E. Wiesel, Professor		22b. TELEPHONE (Include Area Code) (513) 255-4476	22c. OFFICE SYMBOL ENY

UNCLASSIFIED

The purpose of this thesis was to develop a computer program to model the motion and radar beam characteristics of different configurations for the distributed sparse array. The effect of the two-body motion on the beam quality of the array was analyzed. Two groups of arrays, planar and three-dimensional were considered. The planar phased arrays were rectangles and disks, and the other arrays included cones and spheres. The number of emitters in the configurations ranged from five to two hundred.

The beam quality parameter was the half-power beamwidth as determined in discrete directions throughout the hemisphere below the array. An array was considered feasible if the beamwidths degraded only slightly during an orbit.

The most useful configuration was found to be a sphere of randomly spaced emitters because it provided narrow beamwidths in all directions below the array. Because of the motion of the array, the beamwidths changed in a predictable, periodic manner. The half-power beamwidths actually improved in certain directions and only slightly degraded in others. The sphere also required the least number of emitters and could be used at any altitude.

UNCLASSIFIED